ON THE ONE-DIMENSIONAL NONLINEAR STOKES-BRINKMAN EQUATIONS FOR MODELING FLOW IN PCL

SURACHAI PHAENCHAT

A THESIS SUBMITTED IN PARTIAL FULFILLMENT OF THE REQUIREMENT FOR THE DEGREE OF MASTER OF SCIENCE IN APPLIED MATHEMATICS

DEPARTMENT OF MATHEMATICS FACULTY OF SCIENCE
KING MONGKUTS INSTITUTE OF TECHNOLOGY LADKRABANG

2019
KMITL-2019-SC-M-001-030

ON THE ONE-DIMENSIONAL NONLINEAR STOKES-BRINKMAN EQUATIONS FOR MODELING FLOW IN PCL

SURACHAI PHAENCHAT

A THESIS SUBMITTED IN PARTIAL FULFILLMENT OF THE REQUIREMENT FOR THE DEGREE OF MASTER OF SCIENCE IN APPLIED MATHEMATICS

DEPARTMENT OF MATHEMATICS FACULTY OF SCIENCE
KING MONGKUT'S INSTITUTE OF TECHNOLOGY LADKRABANG

2019

KMITL-2019-SC-M-001-030

Thesis Title	On the One-Dimensional Nonlinear Stokes-Brinkman Equations for Modeling Flow in PCL
Student Name	Mr.Surachai Phaenchat
Student ID	60605018
Degree	Master Degree of Science in Applied Mathematics
Department	Mathematics
Year	2019
Thesis Advisor	Asst.Prof.Dr.Kanognudge Wuttanachamsri

Abstract

Nowadays, people have several respiratory diseases. One of the main reasons is the inhalation of strange particles such as dust and harmful smoke particles. When an irritant settles in the human body, goblet cells standing within a surface epithelium secrete mucus to catch those particles and then it forms a mucus layer and lies on the tip of cilia aligned along with the ciliated epithelial cells. Then the mucus is moved out of the body by the movement of the cilia. The layer consisting of the hair-like structures and also a Newtonian fluid under the mucus layer is called Periciliary Layer (PCL). In order to study the velocity of the mucus, in this work, we first focus on the velocity of the fluid in the PCL so that it can be used as a boundary condition of the mucus layer. The Stokes-Brinkman equations embedding a nonlinear term is employed for solving this problem. The velocity of the cilia is also imposed in the model. The nonlinear structure is converted into a linear form by using a classical linearization method. In this research we discretize the model by using a finite element method and provide numerical solutions, the velocity of PCL fluid with the nonlinear Stokes-Brinkman equations, which have a good agreement with exact solution. For the velocity of PCL fluid is close to the velocity of cilia and the velocity of PCL is less than the velocity of cilia, which is in accordance with a physical meaning.

Keywords : Moving Solid Phases, Finite Element Method, Galerkin Method, Nonlinear Stoke-Brinkman Equations.

Acknowledgements

I would like to express my deepest appreciation to all those who provided me the possibility to complete this research. My advisor Asst.Prof.Dr.Kanognudge Wuttanachamsri for accepts me as a student, gives me various knowledge, giving me the skill to write a research. Chairperson, Assoc.Prof.Dr.Montri Maleewong for suggestions and helping to correct the research. Examiner, Dr.Wannaporn Sanprasert for suggestion and give me various knowledge. Miss Wiphada Phaobthong to gives me pictures. My family for encouragement and support me. My classmate for our friendship, supportiveness and helping me find my way through graduate.

Surachai Phaenchat

Table of Contents

List of Tables

Table **Page**

List of Figures

Figure **Page**

Symbols

ρ^l Fluid density $(kg/\mu m^3)$

ε^l Porosity (1)

p Pressure $(g/\mu m/s^2)$

μ Dynamic viscosity $(g/\mu m/s)$

g^l Gravity $(\mu m/s^2)$

$\mathbf{k}^{-1}$ Inverse of the permeability tensor $(1/\mu m^2)$

v^s Velocities of the solid phases $(\mu m/s)$

$\dot{\varepsilon}^l$ Material time derivative of the porosity with respect to the solid phase

Chapter 1

Introduction

In this chapter, we will discuss the research motivation, objective, scopes and benefits of the study.

1.1 Research Motivation

In present days, there are several factors causing respiratory failure in human lungs such as factory pollutions. When people inhale the strange particles into their bodies, they spread directly into the respiratory tracts and lungs. This may cause respiratory diseases such as Pulmonary emphysema, Acute Bronchitis and Pneumonia. Some people who have the respiratory diseases may have shortness of breath, cough and chest tightness. In this study, we focus on fluid flow in the respiratory system.

Figure 1.1 shows a portion of the respiratory tract: trachea, and its cross section.

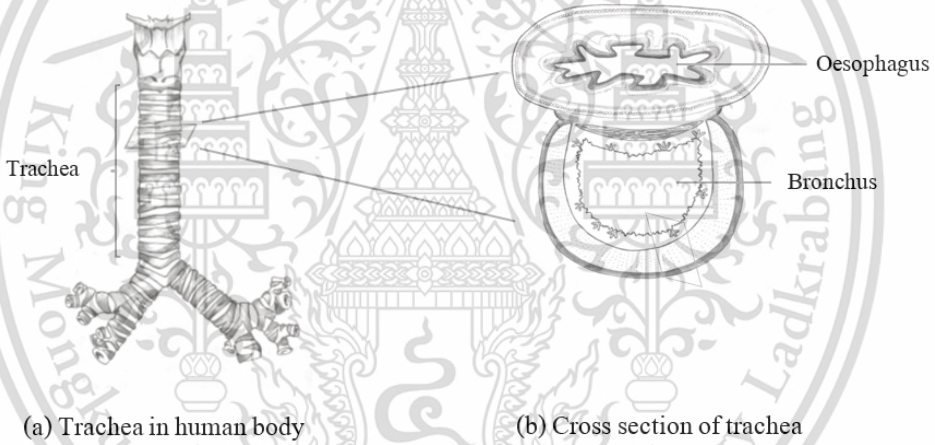

Figure 1.1: Trachea and its cross section.

A sector of the cross section of the trachea is illustrated in Figure 1.2 presenting ciliated cells, hair-like structures, goblet cells and mucus. Among the ciliated cells, there are goblet cells secreting the mucus to trap debris and form a mucus layer on the tip of the hair-like structures. Patients who have respiratory diseases may carry more mucus than usual. The tiny hair-like structures are named cilia, sticking out from the ciliated cells, that are efficiently move back and forward to precede the mucus out the body. The layer containing of cilia and Newtonian fluid is called Periciliary Layer (PCL).

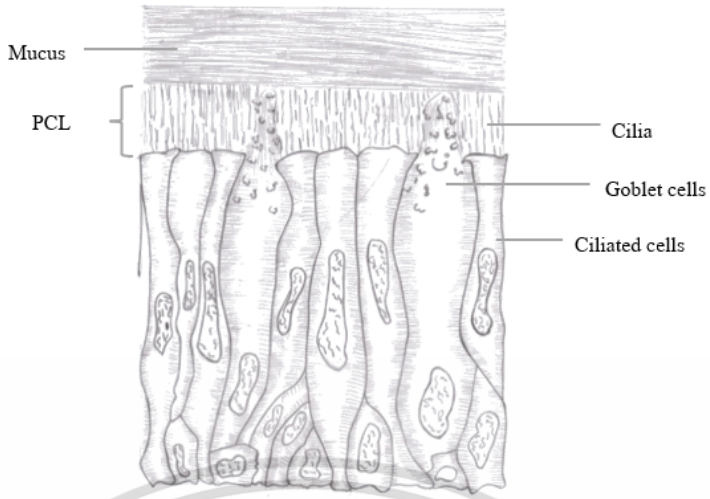

Figure 1.2: Cartoon picture of the portion of the cross section of trachea.

In the PCL, there are both solid phases and cilia. While cilia make angle $\theta = 90°$ with the horizontal plane, we look at this layer as a porous medium as shown in Figure 1.3.

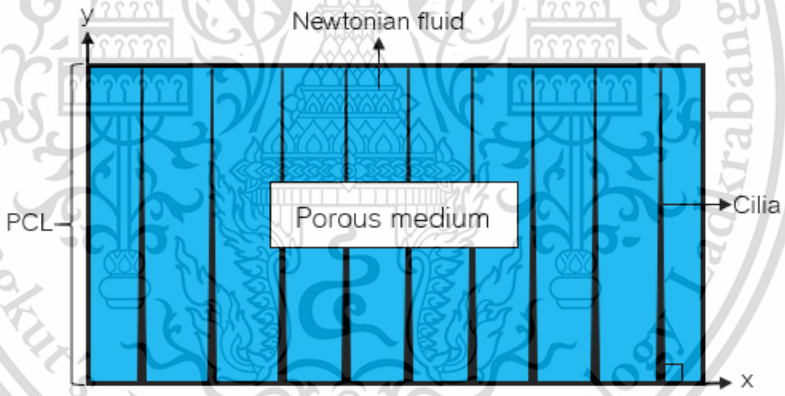

Figure 1.3: Cartoon picture of PCL when cilia are perpendicular to the horizontal plane.

When cilia make angle θ, which is less than $90°$ with the horizontal plane, the PCL can be split into 2 layers, hairy and hairless layers. Hairy layer is viewed as a porous medium and hairless layer is a free-fluid domain as shown in Figure 1.4, when the cilia length is $\xi = y/\sin\theta$. Occasionally, Stokes-Brinkman equations are employed in both domains. The Stokes equation is applied in the free-fluid domain and Brinkman equation is used in the porous medium.

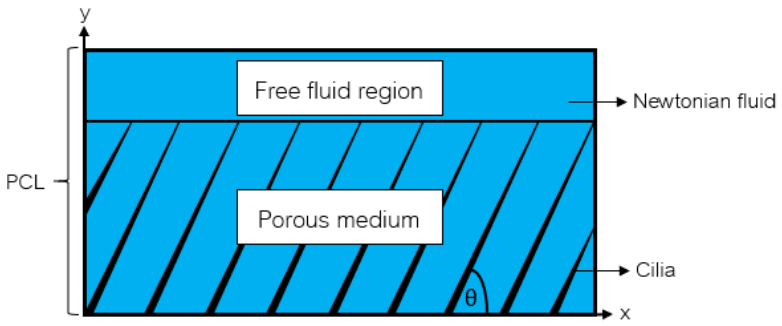

Figure 1.4: The cilia make the angle $\theta < 90^\circ$ with the horizontal plane in PCL.

In this work, we examine the velocity of the fluid in PCL. The Stokes-Brinkman model with a nonlinear term including a moving solid-phase term is employed and discretized by using a finite element method. The nonlinear structure is transformed into a linear form by using a classical linearization method. One of applications is that the velocity of the PCL fluid can be applied to be a boundary condition of the mucus layer. The numerical solutions of the velocities of the PCL fluid are given by using a computer program.

1.2 Objectives of the study

1) To find the velocity of PCL fluid of the nonlinear Strokes-Brinkman equations by using a finite element method.

1.3 Scopes of the study

1) To study the velocity of the PCL fluid by adding nonlinear terms and the cilia velocity in the Stokes-Brinkman equations in one-dimensional domain.

2) To apply the finite element method to the nonlinear Stokes-Brinkman equations in a one-dimensional domain.

1.4 Research methodology

1) Study on the human respiratory system, especially the PCL.

2) Study the nonlinear Stokes-Brinkman equations.

3) Study a finite element methods and solve the governing equation by using a finite element method.

4) Program to find the numerical solutions.

5) Verify the results and conclusion.

6) Summary and write the thesis book.

Table 1.1: Time frame of research.

Activity	Time frame					
	2017	2018				2019
	Oct. - Dec.	Jan. - Mar.	Apr. - Jun.	Jul. - Sep.	Oct. - Jan.	Feb. - May.
Step 1						
Step 2						
Step 3						
Step 4						
Step 5						
Step 6						
step 7						

1.5 Benefit of the study

The result of determining the velocity of PCL fluid can be applied to be a boundary condition of the mucus layer above the cilia to the velocity of mucus in future work.

Chapter 2

Basic knowledge and Literature Reviews

In this chapter, we present the basic knowledge applied to our research as well as the literature reviews.

2.1 Weak Formulation

Suppose that the domain $\Omega = (0, L)$ is divided into N elements. In order to explain the weak formulation, we consider the following sample problem.

$$\begin{aligned} \frac{d^2u}{dx^2} - u = -x, \;\; 0 < x < 1 \\ u(0) = 0, \quad u(1) = 0. \end{aligned} \tag{2.1}$$

Multiplying Eq.(2.1) with a weight function $w \in H_0^1(\Omega)$ and integrating the equation over the domain $\Omega = (0, L)$, we have

$$\int_0^L w \left(\frac{d^2u}{dx^2} - u + x \right) dx = 0. \tag{2.2}$$

Integrating by parts the second order derivative in Eq.(2.2), we have

$$\int_0^L \left(-\frac{dw}{dx}\frac{du}{dx} - wu + wx \right) dx + \left[w\frac{du}{dx} \right]_0^L = 0. \tag{2.3}$$

Eq.(2.3) is called a weak formulation of Eq.(2.1).

2.2 Finite Element Method

The concept of the finite element method is that the solution can be approximated by $\tilde{u}$, which contains unknown coefficients to be determined later such as $\tilde{u} = ax(1-x)$, where a is an unknown constant. The residual is calculated by substituting the trial function into the differential equation. Then, the residual R is

$$R = \frac{d^2\tilde{u}}{dx^2} - \tilde{u} + x = -2a - ax(1-x) + x. \tag{2.4}$$

To determine the unknown constant a. We average the residual over the problem domain and set to be zero. That is,

$$\begin{aligned} I &= \int_0^1 wR dx = \int_0^1 w \left(\frac{d^2\tilde{u}}{dx^2} - \tilde{u} + x \right) dx \\ &= \int_0^1 w[-2a - ax(1-x) + x] dx = 0. \end{aligned} \tag{2.5}$$

There are several methods of weighted residual explained below.

1. Collocation Method: The weight function is defined by Dirac delta function, that is

$$w = \delta(x - x_i), \tag{2.6}$$

where sampling point x_i must be within the domain, $0 < x_i < 1$. Let $x_i = 0.5$, we substitute the weight function into Eq.(2.5), we have $a = 0.2222$. Then, the approximate solution becomes $\tilde{u} = 0.2222x(1-x)$.

2. Least Square Method: The weight function is determined from the residual such that

$$w = \frac{dR}{da}. \tag{2.7}$$

Then, we have $w = -2 - x(1-x)$. Substituting the weight function into Eq.(2.5), we get $a = 0.2305$. Then $\tilde{u} = 0.2305x(1-x)$.

3. Galerkin's method: The weight function is from chosen trial function, that is

$$w = \frac{d\tilde{u}}{da}. \tag{2.8}$$

The weight function of the Galerkin's method is $w = x(1-x)$. Then, we substitute the weight function into Eq.(2.5). Then, we have $a = 0.2272$ so that $\tilde{u} = 0.2272x(1-x)$.

In order to improve the approximate solutions, we can add more terms of the chosen trial function for n unknown constants to be determined as shown in Table 2.1.

Table 2.1: Test Functions for Methods of Weight Residual.

Method	Description
collocation	$w_i = \delta(x - x_i)$, $i = 1, 2, ..., n$, where x_i is a point within the domain
Least Squares	$w_i = \partial R/\partial a_i$, $i = 1, 2, ..., n$, where R is the residual and a_i is an unknown coefficient in the trial function
Galerkin	$w_i = \partial \tilde{u}/\partial a_i$, $i = 1, 2, ..., n$, where $\tilde{u}$ is the selected trial function

2.2.1 Linear Shape Function

In this section, we present linear shape function are used in this research. We consider a subdomain or an element shown in Figure 2.1. One element has two nodes. At each node, the corresponding coordinate value (x_i or x_{i+1}) and the nodal variable (u_i or u_{i+1}) are assigned. Assume the unknown trial function is

$$u = c_1 x + c_2. \tag{2.9}$$

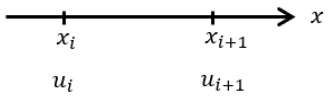

Figure 2.1: A two nodes element.

We next show how to express Eq.(2.9) in terms of nodal variables. We evaluate u at $x = x_i$ and $x = x_{i+1}$. Then

$$u(x_i) = c_1 + c_2 = u_i \tag{2.10}$$

$$u(x_{i+1}) = c_1 x_{i+1} + c_2 = u_{i+1}. \tag{2.11}$$

Solving Eqs.(2.10) and (2.11) to find the values of c_1 and c_2, we have

$$c_1 = \frac{u_{i+1} - u_i}{x_{i+1} - x_i} \tag{2.12}$$

$$c_2 = \frac{u_i x_{i+1} - u_{i+1} x_i}{x_{i+1} - x_i}. \tag{2.13}$$

Substituting Eqs.(4.16) and (4.19) into Eq.(2.9) and rearranging expression, we obtain

$$u = H_1(x) u_i + H_2(x) u_{i+1}, \tag{2.14}$$

or in matrix form

$$u = \begin{bmatrix} H_1 & H_2 \end{bmatrix} \begin{bmatrix} u_i \\ u_{i+1} \end{bmatrix}, \tag{2.15}$$

where

$$H_1 = \frac{x_{i+1} - x}{h_i} \tag{2.16}$$

$$H_2 = \frac{x - x_i}{h_i}, \tag{2.17}$$

and

$$h_i = x_{i+1} - x_i. \tag{2.18}$$

Eq.(2.14) gives an expression in terms of nodal variables. Eqs.(2.16) and (2.17) are called linear shape functions, which are drawn in Figure 2.2.

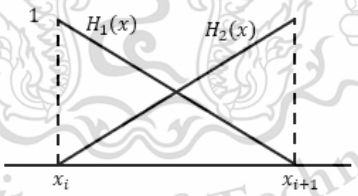

Figure 2.2: Linear shape function.

These functions have the following properties: The shape function $H_1(x)$ has a unit value at node x_i and vanishes at x_{i+1} and $H_2(x)$ has a unit value at node x_{i+1} and vanishes at x_i. That is,

$$\begin{aligned} H_1(x_i) &= 1, \\ H_1(x_{i+1}) &= 0, \\ H_2(x_i) &= 0, \\ H_2(x_{i+1}) &= 1. \end{aligned} \tag{2.19}$$

The sum of all the shape functions is unity, i.e.

$$\sum_{i=1}^{2} H_i(x) = 1 \tag{2.20}$$

2.3 Classical Linearization Method

In this section, we present the classical linearization technique [?]. The basic idea of the classical linearization is to linearize a nonlinear differential equations to be a linear equation. The general form of a differential equation is

$$v^{(n)} + \Re\left(v, v', \ldots, v^{(n-1)}; y\right) + \aleph\left(v, v', \ldots, v^{(n-1)}; y\right) = f(y) \tag{2.21}$$

where $v^{(n)}$ is the n^{th} derivative of v; $\Re$ is the linear differential operator and $\aleph$ is the nonlinear differential operator.

The classical linearization of $\aleph$ is acquired by approximation

$$\aleph \approx \ell^* = \left(\frac{\aleph^*}{\Im^*}\right)\Im, \tag{2.22}$$

where linear differential operator ℓ^* is the function of previous values of v which change during the iteration process; $\aleph^*$ and $\Im^*$ are evaluated from known values of the arguments from previous iterations and $\Im$ is a linear operator. The classical linearization is to change the nonlinear differential equation, Eq.(2.21), to linear differential equation

$$v^{(n)} + \Re(v) + \ell^*(v) = f(y). \tag{2.23}$$

The linear operator $\Im$ may have more than one form of the classical linearization, which is given below, for example,

$$v'v \approx (v')^* v = \Im^* \tag{2.24}$$

$$v'v \approx v^*(v') = \Im^* \tag{2.25}$$

where v^* is approximation of v and $(v')^*$ is the first derivative of approximation of v.

2.4 Literature Reviews

Numerous researchers had concentrated on the PCL [?, ?, ?]. For instance, J. Hussong et al. [?] studied cilia-induced periciliary liquid (PCL) transport measured by means of micro Particle Image Velocimetry (μPIV) with neutrally buoyant tracers. W.L. Lee et al. [?] numerically considered a two-layer Newtonian fluid model consisting of an upper mucus layer and a lower periciliary layer (PCL) to simulate the muco-ciliary transport process. P.G. Jayathilake et al. [?] presented a three-dimensional numerical model to simulate the human pulmonary cilia motion in the PCL. The governing equations were solved using the immersed boundary method combined with the projection method. The numerical results showed the maximum velocity of PCL in a stream-wise direction if cilia had phase differences in both stream-wise and span-wise directions.

In this work, we apply the nonlinear Stokes-Brinkman model to find the velocity of the fluid in PCL. The Stokes-Brinkman equations without the nonlinear term in macroscopic scale had been developed in [?] and proved the well-posedness, when permeability coefficient was considered to be an n-dimensional tensor in [?]. The model

was discretized in an n-dimensional domain in [**?**] by using a mixed finite element method. Next, K. Wuttanachamsri [**?**] employed the Stokes equation to find the mucus velocity by using a mixed finite element method in a three-dimensional domain.

Several literatures had been studied on the porous medium by using Brinkman or Darcy equations [**?**, **?**, **?**, **?**]. For instant, G.N. Gatica et al. [**?**] applied an augmented mixed finite element method to the two-dimensional nonlinear Brinkman model of a porous medium with mixed boundary conditions. S. Suankasem et al. [**?**] used a matched asymptotic expansion to the Brinkman equation and found the velocity of the PCL fluid in a one-dimensional domain. D. Han and X. Wang [**?**] applied the nonlinear Darcy-Brinkman system in the vanishing Darcy number limit and approximated solutions constructed by the method of multiple scale expansion in both space and time. H.N.E. Dine and M. Saad [**?**] proposed a finite volume–finite element scheme based on upstream approach of fractional flow with respect to the gradient of the global pressure. B.K. Jha and M.L. Kaurangini [**?**] presented a new approximated analytical solution for steady flow in parallel-plates channels filled with porous materials governed by non-linear Brinkman-Forchheimer extended Darcy model for three different physical situations and the results were compared with those obtained from an implicit finite-difference solution. M. Ciarletta et al. [**?**] considered the problem of a Brinkman-Forchheimer system to model flow in a porous medium when Newton cooling conditions were applied at the boundary of the body.

However, most of the above literatures studied on static solid phases, except [**?**, **?**, **?**, **?**]. Although K. Chamsri [**?**, **?**], K. Wuttanachamsri [**?**] and S. Suankasem et al. [**?**] worked on moving solid phases, they used only linear models.

In order to study the velocity of the PCL fluid with the nonlinear Stokes-Brinkman equations by using the finite element method, we change the nonlinear term to be linear form by using the classical linearization method. The numerical results are given in Chapter 4.

Chapter 3

Research Methodology

In this chapter, we introduce our governing equations, discretize them by using a finite element method and show how to apply boundary conditions to the stiffness matrix.

3.1 Governing Equation

We present the mathematical model used in this study. We consider this problem in a macroscopic scale where the equations are upscaled by the Hybrid Mixture Theory (HTM) [**?**]. It is an upscaling method that helps to change a microscale equation to a macroscale equation. The macroscopic equation employed in this study is derived from the Navier-Stokes equation in [**?**], which is

$$\frac{\partial}{\partial t}(\rho^l v) + \nabla \cdot \left(\rho^l v \frac{v}{\varepsilon^l}\right) + \varepsilon^l \nabla p - (\mu \Delta v + \mu \nabla(\nabla \cdot v)) - \varepsilon^l \rho^l g^l = -\mu \varepsilon^l \mathbf{k}^{-1} \cdot (v - \varepsilon^l v^s) \tag{3.1}$$

$$\nabla \cdot v = f, \tag{3.2}$$

where $f = \frac{\dot{\varepsilon}^l}{(1-\varepsilon^l)} + \nabla \cdot \varepsilon^l v^s$; ρ^l is the fluid density in the porous medium; v is the multiplication of the fluid velocity with porosity in the PCL; ε^l is the porosity; p is pressure; μ is a dynamic viscosity; g^l is gravity; $\mathbf{k}^{-1}$ is the inverse of the permeability tensor; v^s is the velocities of the solid phases and $\dot{\varepsilon}^l$ is the material time derivative of the porosity with respect to the solid phase, $\dot{\varepsilon}^l = \frac{\partial \varepsilon^l}{\partial t} + v^s \cdot \nabla \varepsilon^l$. Substituting Eq.(3.2) into Eq.(3.1), we have

$$\frac{\partial}{\partial t}(\rho^l v) + \nabla \cdot \left(\rho^l v \frac{v}{\varepsilon^l}\right) + \varepsilon^l \nabla p - (\mu \Delta v + \mu \nabla f) - \varepsilon^l \rho^l g^l = -\mu \varepsilon^l \mathbf{k}^{-1} \cdot (v - \varepsilon^l v^s). \tag{3.3}$$

For one-dimensional domain, Eq.(3.3) can be rewritten as

$$\rho^l \frac{\partial v}{\partial t} + \frac{\rho^l}{\varepsilon^l} \frac{\partial v^2}{\partial y} + \varepsilon^l \frac{\partial p}{\partial x} - \mu \frac{\partial^2 v}{\partial y^2} - \mu \frac{\partial f}{\partial y} - \varepsilon^l \rho^l g^l = -\varepsilon^l \mu k^{-1} \cdot v + \varepsilon^l \mu k^{-1} \cdot (\varepsilon^l v^s), \tag{3.4}$$

where we assume that pressure p change in the x direction and $\frac{\partial p}{\partial x}$ is a constant and the fluid velocity and pressure depend on y direction. Rearranging Eq.(3.4), we have

$$\rho^l \frac{\partial v}{\partial t} + \frac{2\rho^l v}{\varepsilon^l} \frac{\partial v}{\partial y} - \mu \frac{\partial^2 v}{\partial y^2} + \varepsilon^l \mu k^{-1} \cdot v = \varepsilon^l \mu k^{-1} \cdot (\varepsilon^l v^s) + \varepsilon^l \rho^l g^l + \mu \frac{\partial f}{\partial y} - \varepsilon^l \frac{\partial p}{\partial x}, \tag{3.5}$$

where the right hand side terms of the equation are known. In this work, we concentrate on the steady state of Eq.(3.5), which is

$$\frac{2\rho^l v}{\varepsilon^l} \frac{dv}{dy} - \mu \frac{d^2 v}{dy^2} + \varepsilon^l \mu k^{-1} v = (\varepsilon^l)^2 \mu k^{-1} v^s + \varepsilon^l \rho^l g^l + \mu \frac{df}{dy} - \varepsilon^l \frac{dp}{dx}. \tag{3.6}$$

The solid velocity is employed from [**?**], which is a polynomial degree 8 depending on the length of cilia ξ,

$$v^s = c_8\xi^8 + c_7\xi^7 + c_6\xi^6 + c_5\xi^5 + c_4\xi^4 + c_3\xi^3 + c_2\xi^2 + c_1\xi, \tag{3.7}$$

where $\xi = \dfrac{y}{\sin\theta}$ and the variable θ is the angle between the cilia and the horizontal plane. Then, Eq.(3.6) is our governing equation.

3.2 Model Discretization

In this section, we discretize our governing equation provided in Section 3.1 by using the Galerkin finite element method. Since the momentum equation has a nonlinear term, we apply the classical linearization to change it to be linear by substituting Eq.(2.24) into Eq.(3.6). Then, we have

$$\frac{2\rho^l}{\varepsilon^l}(v')^* v - \mu\frac{d^2v}{dy^2} + \varepsilon^l\mu k^{-1}v = \left(\varepsilon^l\right)^2\mu k^{-1}v^s + \varepsilon^l\rho^l g^l + \mu\frac{df}{dy} - \varepsilon^l\frac{dp}{dx}. \tag{3.8}$$

Next, we find the weak formulation of the model by multiplying Eq.(3.8) by a weight function $w \in H_0^1(\Omega)$ and then integrating over the domain $\Omega = (0, L)$. Therefore Eq.(3.8) becomes

$$\begin{aligned}&\int_0^L \left(\frac{2\rho^l}{\varepsilon^l}(v')^* wv - \mu w\frac{d^2v}{dy^2} + \varepsilon^l\mu k^{-1}wv\right)dy \\ &= \int_0^L \left(\left(\varepsilon^l\right)^2\mu k^{-1}v^s w + \varepsilon^l\rho^l g^l w + \mu w\frac{df}{dy} - \varepsilon^l w\frac{dp}{dx}\right)dy.\end{aligned} \tag{3.9}$$

We apply integration by parts to the second order derivative and the term df/dy in Eq. (3.9) and discretize the domain to be n elements. Then, we have

$$\begin{aligned}&\sum_{i=1}^n \int_{y_i}^{y_{i+1}} \left(\frac{2\rho^l}{\varepsilon^l}(v')^* wv + \mu\frac{dw}{dy}\frac{dv}{dy} + \varepsilon^l\mu k^{-1}wv\right)dy \\ &= \sum_{i=1}^n \int_{y_i}^{y_{i+1}} \left(\left(\varepsilon^l\right)^2\mu k^{-1}v^s w + \varepsilon^l\rho^l g^l w - \mu f\frac{dw}{dy} - \varepsilon^l w\frac{dp}{dx}\right)dy + \mu[wf]_0^L + \mu\left[wv'\right]_0^L.\end{aligned} \tag{3.10}$$

Consider the first integration,

$$\int_{y_i}^{y_{i+1}} \left(\frac{2\rho^l}{\varepsilon^l}(v')^* wv + \mu\frac{dw}{dy}\frac{dv}{dy} + \varepsilon^l\mu k^{-1}wv\right)dy. \tag{3.11}$$

We assume that

$$v^* = y.$$

Then

$$(v')^* = 1.$$

Using linear shape functions

$$\begin{aligned}H_1 &= \frac{y_{i+1} - y}{h_i} \\ H_2 &= \frac{y - y_i}{h_i},\end{aligned} \tag{3.12}$$

where $h_i = y_{i+1} - y_i$, we obtain

$$v = H_1 v_1 + H_2 v_2 \tag{3.13}$$

or in the matrix form

$$v = \begin{bmatrix} H_1 & H_2 \end{bmatrix}\begin{bmatrix} v_1 \\ v_2 \end{bmatrix}. \tag{3.14}$$

Replacing the weight function w by the linear shape function Eq.(3.12) and substituing Eq.(3.14) into Eq.(3.11), we have the 2×2 matrix

$$[K_e] = \int_{y_i}^{y_{i+1}} \left(\frac{2\rho^l}{\varepsilon^l} \begin{bmatrix} H_1 \\ H_2 \end{bmatrix} \begin{bmatrix} H_1 & H_2 \end{bmatrix} \begin{bmatrix} v_i \\ v_{i+1} \end{bmatrix} + \mu \begin{bmatrix} H_1' \\ H_2' \end{bmatrix} \begin{bmatrix} H_1' & H_2' \end{bmatrix} \begin{bmatrix} v_i \\ v_{i+1} \end{bmatrix} + \varepsilon^l \mu k^{-1} \begin{bmatrix} H_1 \\ H_2 \end{bmatrix} \begin{bmatrix} H_1 & H_2 \end{bmatrix} \begin{bmatrix} v_i \\ v_{i+1} \end{bmatrix} \right) dy$$

$$[K_e] = \int_{y_i}^{y_{i+1}} \left(\frac{2\rho^l}{\varepsilon^l} \begin{bmatrix} H_1H_1 & H_1H_2 \\ H_2H_1 & H_2H_2 \end{bmatrix} + \mu \begin{bmatrix} H_1'H_1' & H_1'H_2' \\ H_2'H_1' & H_2'H_2' \end{bmatrix} + \varepsilon^l \mu k^{-1} \begin{bmatrix} H_1H_1 & H_1H_2 \\ H_2H_1 & H_2H_2 \end{bmatrix} \right) dy \begin{bmatrix} v_i \\ v_{i+1} \end{bmatrix}.$$

Define

$$[K_e] = \begin{bmatrix} k_{11} & k_{12} \\ k_{21} & k_{22} \end{bmatrix}. \tag{3.15}$$

The elements k_{ij} in $[K_e]$ can be calculated as follows. Consider

$$\begin{aligned}
k_{11} &= \int_{y_i}^{y_{i+1}} \frac{2\rho^l}{\varepsilon^l} H_1H_1 + \mu H_1'H_1' + \varepsilon^l \mu k^{-1} H_1H_1 \, dy \\
&= \int_{y_i}^{y_{i+1}} \frac{2\rho^l}{\varepsilon^l} \left(\frac{y_{i+1} - y}{h_i} \right)^2 + \mu \left(\frac{-1}{h_i} \right)^2 + \varepsilon^l \mu k^{-1} \left(\frac{y_{i+1} - y}{h_i} \right)^2 dy \\
&= \int_{y_i}^{y_{i+1}} \frac{2\rho^l}{\varepsilon^l} \left(\frac{y_{i+1}^2 - 2y_{i+1}y + y^2}{h_i^2} \right) + \left(\frac{\mu}{h_i^2} \right) + \varepsilon^l \mu k^{-1} \left(\frac{y_{i+1}^2 - 2y_{i+1}y + y^2}{h_i^2} \right) dy \\
&= \frac{2\rho^l}{\varepsilon^l h_i^2} \left(y_{i+1}^2 y - 2y_{i+1} \frac{y^2}{2} + \frac{y^3}{3} \right) \Bigg|_{y_i}^{y_{i+1}} + \left(\frac{\mu}{h_i^2} \right) (y) \Bigg|_{y_i}^{y_{i+1}} + \frac{\varepsilon^l \mu k^{-1}}{h_i^2} \left(y_{i+1}^2 y - 2y_{i+1} \frac{y^2}{2} + \frac{y^3}{3} \right) \Bigg|_{y_i}^{y_{i+1}} \\
&= \frac{2\rho^l}{\varepsilon^l h_i^2} \left(\frac{y_{i+1}^3 - 3y_{i+1}^2 y_i + 3y_{i+1}y_i^2 - y_i^3}{3} \right) + \frac{\mu}{h_i^2} (y_{i+1} - y_i) \\
&+ \frac{\varepsilon^l \mu k^{-1}}{h_i^2} \left(\frac{y_{i+1}^3 - 3y_{i+1}^2 y_i + 3y_{i+1}y_i^2 - y_i^3}{3} \right) \\
&= \frac{2\rho^l}{\varepsilon^l h_i^2} \left(\frac{(y_{i+1} - y_i)^3}{3} \right) + \frac{\mu}{h_i^2} (y_{i+1} - y_i) + \frac{\varepsilon^l \mu k^{-1}}{h_i^2} \left(\frac{(y_{i+1} - y_i)^3}{3} \right) \\
&= \frac{2\rho^l}{\varepsilon^l h_i^2} \left(\frac{h_i^3}{3} \right) + \frac{\mu}{h_i^2} (h_i) + \frac{\varepsilon^l \mu k^{-1}}{h_i^2} \left(\frac{h_i^3}{3} \right) \\
&= \frac{2\rho^l h_i}{3\varepsilon^l} + \frac{\mu}{h_i} + \frac{\varepsilon^l \mu k^{-1} h_i}{3}.
\end{aligned}$$

Thus,

$$k_{11} = \frac{2\rho^l h_i}{3\varepsilon^l} + \frac{\mu}{h_i} + \frac{\varepsilon^l \mu k^{-1} h_i}{3}. \tag{3.16}$$

Consider

$$\begin{aligned}
k_{12} &= \int_{y_i}^{y_{i+1}} \frac{2\rho^l}{\varepsilon^l} H_1H_2 + \mu H_1'H_2' + \varepsilon^l \mu k^{-1} H_1H_2 \, dy \\
&= \int_{y_i}^{y_{i+1}} \frac{2\rho^l}{\varepsilon^l} \left(\frac{y_{i+1} - y}{h_i} \right) \left(\frac{y - y_i}{h_i} \right) + \mu \left(\frac{-1}{h_i} \right) \left(\frac{1}{h_i} \right) + \varepsilon^l \mu k^{-1} \left(\frac{y_{i+1} - y}{h_i} \right) \left(\frac{y - y_i}{h_i} \right) dy \\
&= \int_{y_i}^{y_{i+1}} \frac{2\rho^l}{\varepsilon^l} \left(\frac{y_{i+1}y - y_{i+1}y_i - y^2 + y_iy}{h_i^2} \right) - \left(\frac{\mu}{h_i^2} \right) + \varepsilon^l \mu k^{-1} \left(\frac{y_{i+1}y - y_{i+1}y_i - y^2 + y_iy}{h_i^2} \right) dy
\end{aligned}$$

$$
\begin{aligned}
k_{12} &= \frac{2\rho^l}{\varepsilon^l h_i^2}\left(y_{i+1}\frac{y^2}{2} - y_{i+1}y_i y - \frac{y^3}{3} + y_i\frac{y^2}{2}\right)\Bigg|_{y_i}^{y_{i+1}} - \left(\frac{\mu}{h_i^2}\right)(y)\Big|_{y_i}^{y_{i+1}} \\
&+ \frac{\varepsilon^l\mu k^{-1}}{h_i^2}\left(y_{i+1}\frac{y^2}{2} - y_{i+1}y_i y - \frac{y^3}{3} + y_i\frac{y^2}{2}\right)\Bigg|_{y_i}^{y_{i+1}} \\
&= \frac{2\rho^l}{\varepsilon^l h_i^2}\left(\frac{y_{i+1}^3}{2} - y_{i+1}^2 y_i - \frac{y_{i+1}^3}{3} + y_i\frac{y_{i+1}^2}{2} - y_{i+1}\frac{y_i^2}{2} + y_{i+1}y_i^2 + \frac{y_i^3}{3} - \frac{y_i^3}{2}\right) - \frac{\mu}{h_i^2}(y_{i+1} - y_i) \\
&+ \frac{\varepsilon^l\mu k^{-1}}{h_i^2}\left(\frac{y_{i+1}^3}{2} - y_{i+1}^2 y_i - \frac{y_{i+1}^3}{3} + y_i\frac{y_{i+1}^2}{2} - y_{i+1}\frac{y_i^2}{2} + y_{i+1}y_i^2 + \frac{y_i^3}{3} - \frac{y_i^3}{2}\right) \\
&= \frac{2\rho^l}{\varepsilon^l h_i^2}\left(\frac{y_{i+1}^3 - 3y_{i+1}^2 y_i + 3y_{i+1}y_i^2 - y_i^3}{6}\right) - \frac{\mu}{h_i^2}(y_{i+1} - y_i) \\
&+ \frac{\varepsilon^l\mu k^{-1}}{h_i^2}\left(\frac{y_{i+1}^3 - 3y_{i+1}^2 y_i + 3y_{i+1}y_i^2 - y_i^3}{6}\right) \\
&= \frac{2\rho^l}{\varepsilon^l h_i^2}\left(\frac{(y_{i+1} - y_i)^3}{6}\right) - \frac{\mu}{h_i^2}(y_{i+1} - y_i) + \frac{\varepsilon^l\mu k^{-1}}{h_i^2}\left(\frac{(y_{i+1} - y_i)^3}{6}\right) \\
&= \frac{2\rho^l}{\varepsilon^l h_i^2}\left(\frac{h_i^3}{6}\right) - \frac{\mu}{h_i^2}(h_i) + \frac{\varepsilon^l\mu k^{-1}}{h_i^2}\left(\frac{h_i^3}{6}\right) \\
&= \frac{\rho^l h_i}{3\varepsilon^l} - \frac{\mu}{h_i} + \frac{\varepsilon^l\mu k^{-1}h_i}{6}.
\end{aligned}
$$

Thus,

$$k_{12} = \frac{\rho^l h_i}{3\varepsilon^l} - \frac{\mu}{h_i} + \frac{\varepsilon^l\mu\mathbf{k}^{-1}h_i}{6} = k_{21}. \tag{3.17}$$

and

$$
\begin{aligned}
k_{22} &= \int_{y_i}^{y_{i+1}} \frac{2\rho^l}{\varepsilon^l}H_2H_2 + \mu H_2'H_2' + \varepsilon^l\mu k^{-1}H_2H_2\ dy \\
&= \int_{y_i}^{y_{i+1}} \frac{2\rho^l}{\varepsilon^l}\left(\frac{y - y_i}{h_i}\right)^2 + \mu\left(\frac{1}{h_i}\right)^2 + \varepsilon^l\mu k^{-1}\left(\frac{y - y_i}{h_i}\right)^2 dy \\
&= \int_{y_i}^{y_{i+1}} \frac{2\rho^l}{\varepsilon^l}\left(\frac{y^2 - 2yy_i + y_i^2}{h_i^2}\right) + \left(\frac{\mu}{h_i^2}\right) + \varepsilon^l\mu k^{-1}\left(\frac{y^2 - 2yy_i + y_i^2}{h_i^2}\right) dy \\
&= \frac{2\rho^l}{\varepsilon^l h_i^2}\left(\frac{y^3}{3} - 2\frac{y^2}{2}y_i + y_i^2 y\right)\Bigg|_{y_i}^{y_{i+1}} + \left(\frac{\mu}{h_i^2}\right)(y)\Big|_{y_i}^{y_{i+1}} + \frac{\varepsilon^l\mu k^{-1}}{h_i^2}\left(\frac{y^3}{3} - 2\frac{y^2}{2}y_i + y_i^2 y\right)\Bigg|_{y_i}^{y_{i+1}} \\
&= \frac{2\rho^l}{\varepsilon^l h_i^2}\left(\frac{y_{i+1}^3 - 3y_{i+1}^2 y_i + 3y_{i+1}y_i^2 - y_i^3}{3}\right) + \frac{\mu}{h_i^2}(y_{i+1} - y_i) \\
&+ \frac{\varepsilon^l\mu k^{-1}}{h_i^2}\left(\frac{y_{i+1}^3 - 3y_{i+1}^2 y_i + 3y_{i+1}y_i^2 - y_i^3}{3}\right) \\
&= \frac{2\rho^l}{\varepsilon^l h_i^2}\left(\frac{(y_{i+1} - y_i)^3}{3}\right) + \frac{\mu}{h_i^2}(y_{i+1} - y_i) + \frac{\varepsilon^l\mu k^{-1}}{h_i^2}\left(\frac{(y_{i+1} - y_i)^3}{3}\right) \\
&= \frac{2\rho^l}{\varepsilon^l h_i^2}\left(\frac{h_i^3}{3}\right) + \frac{\mu}{h_i^2}(h_i) + \frac{\varepsilon^l\mu k^{-1}}{h_i^2}\left(\frac{h_i^3}{3}\right) \\
&= \frac{2\rho^l h_i}{3\varepsilon^l} + \frac{\mu}{h_i} + \frac{\varepsilon^l\mu k^{-1}h_i}{3}.
\end{aligned}
$$

Thus,

$$k_{22} = \frac{2\rho^l h_i}{3\varepsilon^l} + \frac{\mu}{h_i} + \frac{\varepsilon^l\mu k^{-1}h_i}{3}. \tag{3.18}$$

Next, we consider the right hand side terms of Eq.(3.10):

$$\sum_{i=1}^{n}\int_{y_i}^{y_{i+1}}\left(\left(\varepsilon^l\right)^2\mu k^{-1}v^s w + \varepsilon^l\rho^l g^l w - \mu f\frac{dw}{dy} - \varepsilon^l w\frac{dp}{dx}\right)dy + \mu[wf]_0^L + \mu\left[wv'\right]_0^L. \tag{3.19}$$

Define the vector

$$[F_e] = \int_{y_i}^{y_{i+1}} \left(\left(\varepsilon^l\right)^2 \mu k^{-1} v^s \begin{bmatrix} H_1 \\ H_2 \end{bmatrix} + \varepsilon^l \rho^l g^l \begin{bmatrix} H_1 \\ H_2 \end{bmatrix} + \mu f \begin{bmatrix} H_1' \\ H_2' \end{bmatrix} - \varepsilon^l \frac{dp}{dx} \begin{bmatrix} H_1 \\ H_2 \end{bmatrix} \right) dy + \mu \left[f \begin{bmatrix} H_1 \\ H_2 \end{bmatrix} \right]_0^L + \mu \left[v' \begin{bmatrix} H_1 \\ H_2 \end{bmatrix} \right]_0^L, \tag{3.20}$$

where the variables in Eq.(3.20) are known which can be calculated by coding in a computer program. Then, the stiffness matrix of Eq.(3.10) is

$$[K]\{v\} = [F] \tag{3.21}$$

where $[K]$ and $[F]$ are assembly $n \times n$ matrix and $n \times 1$ vector, respectively, and {v} is a $n \times 1$ vector. We find the Darcy velocity of PCL fluid or v by using a computer program.

3.3 Boundary Conditions

In this section, we assume that the velocity of the PCL fluid at the base of the cilia is zero and the velocity at the tip of cilia is that the rate of change with respect to y is equal to zero. That is $v(0) = 0$ and $v'(L) = 0$. To apply the boundary conditions to the stiffness matrix by using Eq.(3.20), we consider the boundary terms

$$\begin{aligned} \mu \left[f \begin{bmatrix} H_1 \\ H_2 \end{bmatrix} \right]_0^L + \mu \left[v' \begin{bmatrix} H_1 \\ H_2 \end{bmatrix} \right]_0^L &= \mu \left\{ f(L) \begin{bmatrix} H_1(L) \\ H_2(L) \end{bmatrix} - f(0) \begin{bmatrix} H_1(0) \\ H_2(0) \end{bmatrix} \right\} \\ &\quad + \mu \left\{ v'(L) \begin{bmatrix} H_1(L) \\ H_2(L) \end{bmatrix} - v'(0) \begin{bmatrix} H_1(0) \\ H_2(0) \end{bmatrix} \right\} \\ &= \mu \left\{ f(L) \begin{bmatrix} 0 \\ 1 \end{bmatrix} - f(0) \begin{bmatrix} 1 \\ 0 \end{bmatrix} \right\} + \mu \left\{ v'(L) \begin{bmatrix} 0 \\ 1 \end{bmatrix} - v'(0) \begin{bmatrix} 1 \\ 0 \end{bmatrix} \right\} \\ &= \mu \left\{ \begin{bmatrix} -f(0) \\ f(L) \end{bmatrix} \right\} + \mu \left\{ \begin{bmatrix} -v'(0) \\ v'(L) \end{bmatrix} \right\}. \end{aligned}$$

Then, we can apply the boundary conditions to the stiffness matrix as follows.

$$\begin{bmatrix} k_{11} & k_{12} & \cdots & k_{1n} \\ k_{21} & k_{22} & \cdots & k_{2n} \\ \vdots & \vdots & \ddots & \vdots \\ k_{n1} & k_{n2} & \cdots & k_{nn} \end{bmatrix} \begin{Bmatrix} v_1 \\ v_2 \\ \vdots \\ v_n \end{Bmatrix} = \begin{bmatrix} F_1 - \mu f(0) - \mu v'(0) \\ F_2 \\ \vdots \\ F_n + \mu f(L) + \mu v'(L) \end{bmatrix}. \tag{3.22}$$

Since, the velocity of the PCL fluid at the bottom of our domain is zero or $v(0) = 0$, we have

$$\begin{bmatrix} 1 & 0 & \cdots & 0 \\ k_{21} & k_{22} & \cdots & k_{2n} \\ \vdots & \vdots & \ddots & \vdots \\ k_{n1} & k_{n2} & \cdots & k_{nn} \end{bmatrix} \begin{Bmatrix} v_1 \\ v_2 \\ \vdots \\ v_n \end{Bmatrix} = \begin{bmatrix} 0 \\ F_2 \\ \vdots \\ F_n + \mu f(L) + \mu v'(L) \end{bmatrix}. \tag{3.23}$$

Chapter 4

Numerical Results

In this chapter, we find the velocity of PCL fluid by using a computer program to solve the problems in both, linear and nonlinear equations. The linear equation is solved because we need to verify and compare our numerical solutions with an exact solution. In the nonlinear section, to verify the numerical results, we compare our numerical solutions with the velocity of cilia when cilia make angle $\theta = 50°, 60°, ..., 90°$ with the horizontal plane. The constant values in the Stokes-Brinkman equations are obtained from [**?**], which are $\rho^l = 992.2 \times 10^{-15}$; $g^l = 9.81 \times 10^{-6}$; $\partial p/\partial x = -1 \times 10^{-9}$; $\varepsilon^l = 0.7987$; $\mu = 3 \times 10^{-6}$, $k^{-1} = 474.0841$ and c_i are shown in Table 4.1, $i = 1, 2, .., 8$.

Table 4.1: The eighth-order polynomial functions: $c_8\xi^8 + c_7\xi^7 + c_6\xi^6 + c_5\xi^5 + c_4\xi^4 + c_3\xi^3 + c_2\xi^2 + c_1\xi$ approximating the speed along a cilium for angles $50°, 60°, ..., 90°$.

Coefficient	degree				
$10^5\times$	$50°$	$60°$	$70°$	$80°$	$90°$
c_8	0.2498	0.4043	-0.4987	-0.3648	-0.5386
c_7	-1.0781	-1.6788	2.1268	1.5687	2.2148
c_6	1.9290	2.8656	-3.7102	-2.7659	-3.7309
c_5	-1.8459	-2.5945	3.4021	2.5751	3.3198
c_4	1.0133	1.3380	-1.7529	-1.3584	-1.6788
c_3	-0.3157	-0.3896	0.5012	0.4022	0.4803
c_2	0.0504	0.0585	-0.0717	-0.0593	-0.0694
c_1	-0.0023	-0.0024	0.0049	0.0044	0.0050

4.1 Exact Solution of Stokes-Brinkman Equations

In this section, we provide the exact solution of the Stokes-Brinkman equations without the nonlinear term, the velocity of cilia, and gravity. Then our governing Eq.(3.6) becomes

$$\varepsilon^l \frac{dp}{dx} = \mu \frac{d^2v}{dy^2} - \varepsilon^l \mu k^{-1} v. \tag{4.1}$$

Dividing Eq.(4.1) both sides by ε^l, we have

$$\frac{dp}{dx} = \mu/\varepsilon^l \frac{d^2v}{dy^2} - \mu k^{-1} v, \tag{4.2}$$

where here we assume that the boundary conditions are

$$v(d) = v_0 \text{ and } v(0) = 0. \tag{4.3}$$

where d and v_0 are constants.

To find the analytical solution that satisfies the specific boundary conditions. We first examine the general solution of Eq.(4.1), where its auxiliary equation is

$$\frac{\mu}{\varepsilon^l}m^2 - \left(\mu k^{-1}\right) = 0. \tag{4.4}$$

(4.5)

Dividing μ both side, we have

$$\left(\frac{1}{\varepsilon^l}\right)m^2 - k^{-1} = 0. \tag{4.6}$$

Then, we obtain

$$m = \pm\sqrt{\varepsilon^l k^{-1}}. \tag{4.7}$$

Thus the general solution is

$$v_c = c_1 e^{y\sqrt{\varepsilon^l k^{-1}}} + c_2 e^{-y\sqrt{\varepsilon^l k^{-1}}}. \tag{4.8}$$

Next, we find the particular solution. That is

$$v_p = A, \tag{4.9}$$

$$v_p' = 0, \tag{4.10}$$

$$v_p'' = 0, \tag{4.11}$$

where A is a constant. Substituting Eqs.(4.9) and (4.11) into Eq.(4.1), we obtain

$$\begin{aligned} -\mu k^{-1}A &= \frac{dp}{dx}, \\ A &= -\frac{1}{\mu k^{-1}}\frac{dp}{dx}. \end{aligned} \tag{4.12}$$

Thus,

$$v_p = -\frac{1}{\mu k^{-1}}\frac{dp}{dx}. \tag{4.13}$$

Therefore, $v = v_c + v_p$, we have

$$v(y) = c_1 e^{y\sqrt{\varepsilon^l k^{-1}}} + c_2 e^{-y\sqrt{\varepsilon^l k^{-1}}} - \frac{1}{\mu k^{-1}}\frac{dp}{dx}. \tag{4.14}$$

To find c_1 and c_2, we apply the boundary conditions Eq.(4.3) to Eq.(4.14). Then

$$0 = v(0) = c_1 e^{0\sqrt{\varepsilon^l k^{-1}}} + c_2 e^{0\sqrt{\varepsilon^l k^{-1}}} - \frac{1}{\mu k^{-1}}\frac{dp}{dx}. \tag{4.15}$$

Thus,

$$c_1 = -c_2 + \frac{1}{\mu k^{-1}}\frac{dp}{dx}, \tag{4.16}$$

and

$$v_0 = v(d) = c_1 e^{d\sqrt{\varepsilon^l k^{-1}}} + c_2 e^{-d\sqrt{\varepsilon^l k^{-1}}} - \frac{1}{\mu k^{-1}}\frac{dp}{dx}. \tag{4.17}$$

Substituting Eq.(4.16) into Eq.(4.17), we have

$$v_0 = \left(-c_2 + \frac{1}{\mu k^{-1}}\frac{dp}{dx}\right)e^{d\sqrt{\varepsilon^l k^{-1}}} + c_2 e^{-d\sqrt{\varepsilon^l k^{-1}}} - \frac{1}{\mu k^{-1}}\frac{dp}{dx}. \tag{4.18}$$

Thus,

$$c_2 = \frac{v_0}{e^{-d\sqrt{\varepsilon^l k^{-1}}} - e^{d\sqrt{\varepsilon^l k^{-1}}}} - \frac{1}{\mu k^{-1}} \frac{dp}{dx} \left(\frac{e^{d\sqrt{\varepsilon^l k^{-1}}} - 1}{e^{-d\sqrt{\varepsilon^l k^{-1}}} - e^{d\sqrt{\varepsilon^l k^{-1}}}} \right). \tag{4.19}$$

Substituting Eq.(4.19) into Eq.(4.16), we obtain

$$c_1 = \frac{-v_0}{e^{-d\sqrt{\varepsilon^l k^{-1}}} - e^{d\sqrt{\varepsilon^l k^{-1}}}} + \frac{1}{\mu k^{-1}} \frac{dp}{dx} \left(\frac{e^{d\sqrt{\varepsilon^l k^{-1}}} - 1}{e^{-d\sqrt{\varepsilon^l k^{-1}}} - e^{d\sqrt{\varepsilon^l k^{-1}}}} \right) + \frac{1}{\mu k^{-1}} \frac{dp}{dx}. \tag{4.20}$$

Substituting Eqs.(4.19) and (4.20) into Eq.(4.14), we have

$$\begin{aligned} v(y) = &\left[\frac{-v_0}{e^{-d\sqrt{\varepsilon^l k^{-1}}} - e^{d\sqrt{\varepsilon^l k^{-1}}}} + \frac{1}{\mu k^{-1}} \frac{dp}{dx} \left(\frac{e^{d\sqrt{\varepsilon^l k^{-1}}} - 1}{e^{-d\sqrt{\varepsilon^l k^{-1}}} - e^{d\sqrt{\varepsilon^l k^{-1}}}} \right) + \frac{1}{\mu k^{-1}} \frac{dp}{dx} \right] e^{y\sqrt{\varepsilon^l k^{-1}}} \\ &+ \left[\frac{v_0}{e^{-d\sqrt{\varepsilon^l k^{-1}}} - e^{d\sqrt{\varepsilon^l k^{-1}}}} - \frac{1}{\mu k^{-1}} \frac{dp}{dx} \left(\frac{e^{d\sqrt{\varepsilon^l k^{-1}}} - 1}{e^{-d\sqrt{\varepsilon^l k^{-1}}} - e^{d\sqrt{\varepsilon^l k^{-1}}}} \right) \right] e^{-y\sqrt{\varepsilon^l k^{-1}}} - \frac{1}{\mu k^{-1}} \frac{dp}{dx}. \end{aligned} \tag{4.21}$$

Rearranging Eq.(4.21). we obtain the analytical solution that satisfies with the boundary conditions

$$\begin{aligned} v(y) = &v_0 \left(\frac{e^{-y\sqrt{\varepsilon^l k^{-1}}} - e^{y\sqrt{\varepsilon^l k^{-1}}}}{e^{-d\sqrt{\varepsilon^l k^{-1}}} - e^{d\sqrt{\varepsilon^l k^{-1}}}} \right) + \frac{1}{\mu k^{-1}} \frac{dp}{dx} \left(\frac{e^{(y+d)\sqrt{\varepsilon^l k^{-1}}} - e^{(d-y)\sqrt{\varepsilon^l k^{-1}}} - e^{y\sqrt{\varepsilon^l k^{-1}}} + e^{-y\sqrt{\varepsilon^l k^{-1}}}}{e^{-d\sqrt{\varepsilon^l k^{-1}}} - e^{d\sqrt{\varepsilon^l k^{-1}}}} \right) \\ &+ \frac{1}{\mu k^{-1}} \frac{dp}{dx} \left(e^{y\sqrt{\varepsilon^l k^{-1}}} - 1 \right). \end{aligned} \tag{4.22}$$

4.2 Numerical Result of the Stokes-Brinkman Equations

We apply the finite element technique to the Stokes-Brinkman equations without nonlinear term and velocity of cilia in Eq.(3.21) to find the velocity of PCL fluid. The numerical result is compared with the exact solutions, Eq.(4.22), as shown in Figure 4.1, where the boundary conditions are $v(0) = 0$ and $v'(1) = 1$.

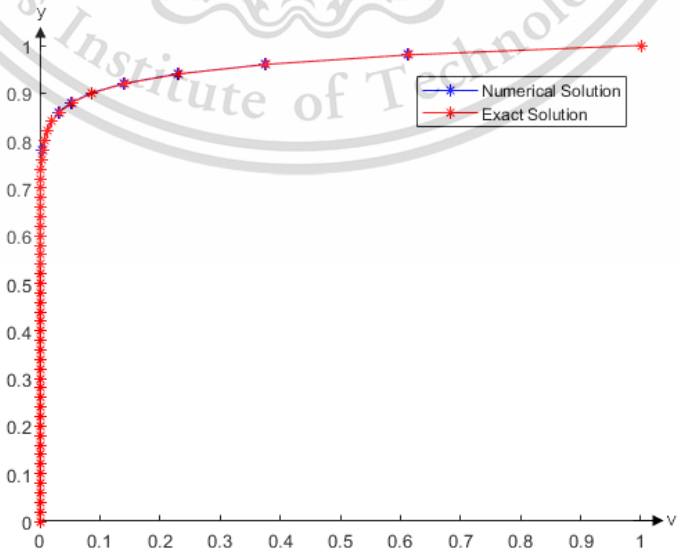

Figure 4.1: The velocity of PCL fluid when $\theta = 90°$ for the Stokes-Brinkman equations.

We calculate the Stokes-Brinkman equations for 50 elements. Figure 4.1 shows that the velocity of the PCL fluid is almost unchanged when $y \leqslant 0.8$, but when $y > 0.8$ the velocity of the PCL fluid is increases rapidly. The pointwise of the numerical and exact solutions are shown in Table 4.2, in which we show the values only at $y = 0, 0.2, ..., 1$. The l_2-norm error of the 50 elements is 0.0072. Then, the numerical result is in a good agreement with the exact solution.

Table 4.2: Pointwise numerical and exact solutions at $y = 0, 0.2, ..., 1$.

y	0.0	0.2	0.4	0.6	0.8	1.0
Numerical	0.0	7.0080×10^{-7}	1.0894×10^{-6}	5.3748×10^{-5}	0.0073	1.0
Exact	0.0	3.4303×10^{-9}	4.4822×10^{-7}	5.8568×10^{-5}	0.0077	1.0

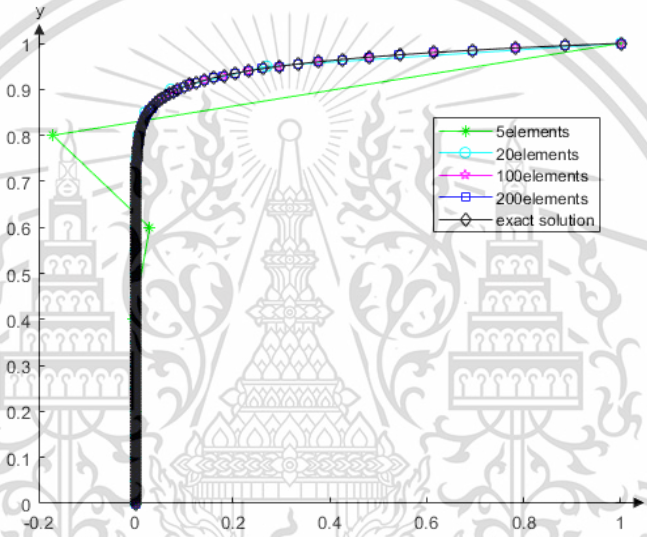

Figure 4.2: The velocity of PCL fluid when $\theta = 90°$ for 5, 20, 100 and 200 elements of the Stokes-Brinkman equations.

Figure 4.2 shows the numerical of 5, 20, 100 and 200 elements. Notice that when the number of elements increases, the solution convert to exact solution. The l_2-norm error of the solution for 5, 20, 100 and 200 elements are shown in Table 4.3.

Table 4.3: The l_2-norm error of the numerical solutions for 5, 20, 100 and 200 elements.

Number of elements	l_2-norm error
5	0.1808
20	0.0302
100	0.0025
200	0.0008

Table 4.3 shows the l_2-norm error of the numerical solutions which four different number of elements, which are 5,20,100 and 200 elements. It's obvious from the Table that the more number of elements we use, the less of the errors we obtain.

4.3 Numerical Results of Nonlinear Stokes-Brinkman Equations

We apply the finite element technique to the nonlinear Stokes-Brinkman equations to find the velocity of PCL fluid when cilia make angle, $\theta = 50°, 60°, ..., 90°$, with the horizontal plane. The numerical results are compared with the velocity of cilia for $\theta = 50°, 60°, ..., 90°$ as shown in Figures 4.3 to 4.12 with the boundary conditions $v(0) = 0$ and $v'(L) = 0$ where L is height from base of cilia to tip of cilia when the cilia make angle θ with horizontal plane. That is the boundary conditions $v(0) = 0$ and $v'(\sin\theta) = 0$ because we assume that the length of cilia is one. Figures 4.3, 4.5, 4.7, 4.9 and 4.11 illustrate Darcy velocity, $v = \varepsilon^l v^l$ of PCL fluid for the angles $50°, 60°, 70°, 80°$ and $90°$, respectively, while Figures 4.4, 4.6, 4.8, 4.10 and 4.12 show the velocity, $v^l = v/\varepsilon^l$, of the PCL fluid for angles $50°, 60°, 70°, 80°$ and $90°$, respectively. We calculate the nonlinear Stokes-Brinkman equation for 50 elements. The pointwise of the numerical solutions and the velocity of cilia values are shown in Tables 4.4 to 4.12. The l_2-norm error of the 50 elements of the numerical solutions when cilia make angle $\theta = 50°, 60°, ..., 90°$ are shown in Table 4.9.

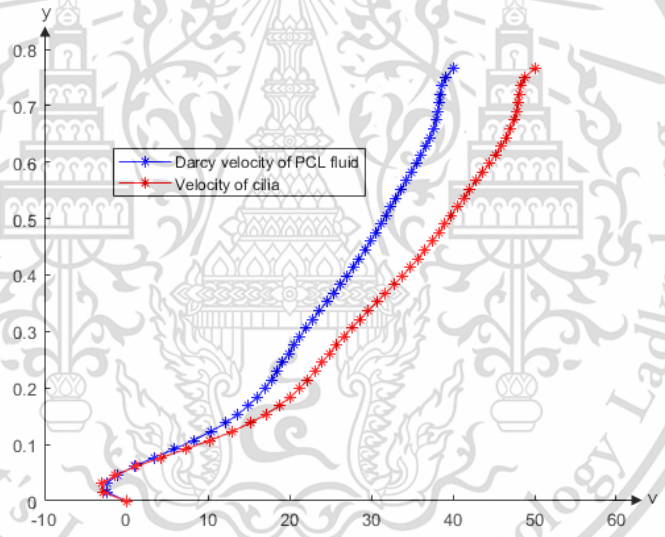

Figure 4.3: The Darcy velocity of the PCL fluid and the cilia velocity when $\theta = 50°$.

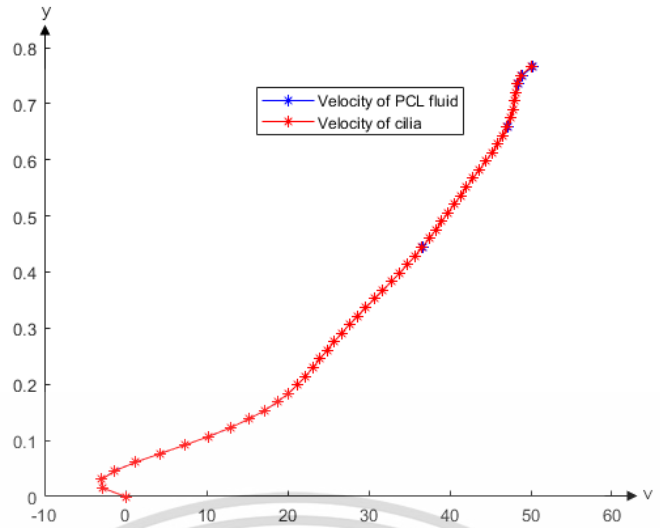

Figure 4.4: The velocity of the PCL fluid and the cilia velocity when $\theta = 50°$.

Table 4.4: Pointwise numerical solution and the velocity of cilia when cilia make angle $\theta = 50°$ with the horizontal plane.

y	0	0.1532	0.3064	0.4596	0.6128	0.7660
Numerical result	0	17.1404	27.6199	37.4526	45.2197	50.1869
Velocity of cilia	0	17.1287	27.6197	37.4500	45.2072	50

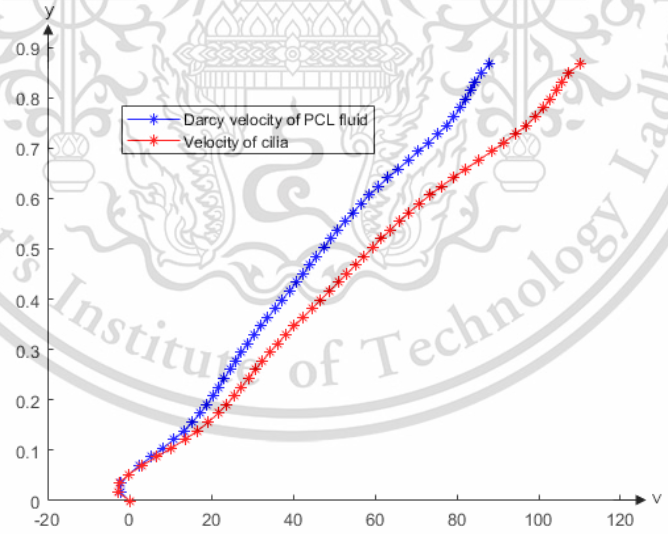

Figure 4.5: The Darcy velocity of the PCL fluid and the cilia velocity when $\theta = 60°$.

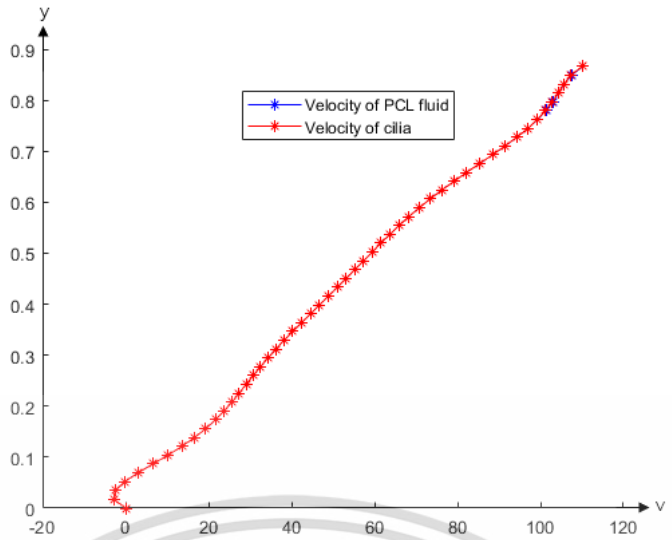

Figure 4.6: The velocity of PCL the fluid and the cilia velocity when $\theta = 60°$.

Table 4.5: Pointwise numerical solution and the velocity of cilia when cilia make angle $\theta = 60°$ with the horizontal plane.

y	0	0.1732	0.3464	0.5196	0.6928	0.8660
Numerical result	0	21.6811	40.2606	61.5305	88.4209	110.1869
Velocity of cilia	0	21.6704	40.2633	61.5345	88.4092	110

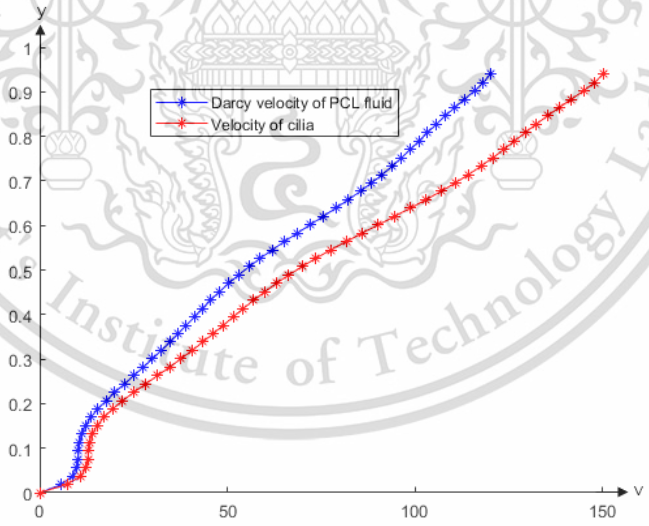

Figure 4.7: The Darcy velocity of the PCL fluid and the cilia velocity when $\theta = 70°$.

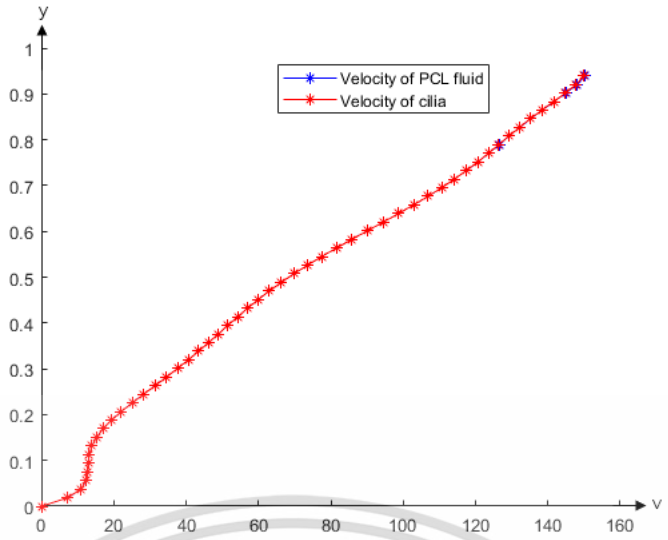

Figure 4.8: The velocity of the PCL fluid and the cilia velocity when $\theta = 70°$.

Table 4.6: Pointwise numerical solution and the velocity of cilia when cilia make angle $\theta = 70°$ with the horizontal plane.

y	0	0.1879	0.3759	0.5638	0.7518	0.9397
Numerical result	0	19.3935	48.8792	81.6042	120.6487	150.2675
Velocity of cilia	0	19.4125	48.8805	81.6108	120.6330	150

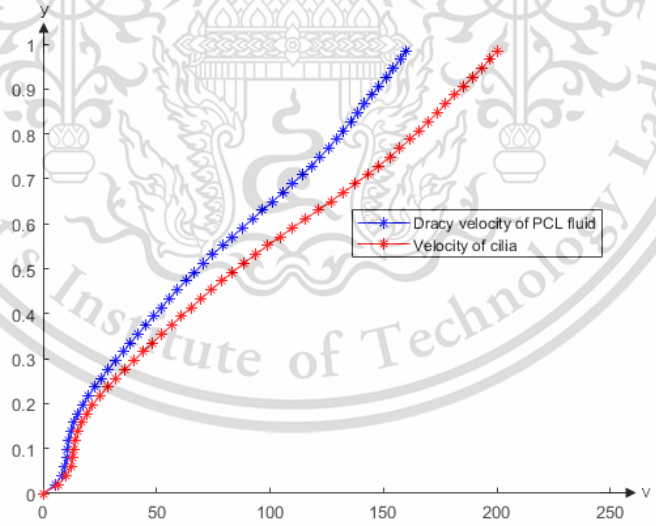

Figure 4.9: The Darcy velocity of the PCL fluid and the cilia velocity when $\theta = 80°$.

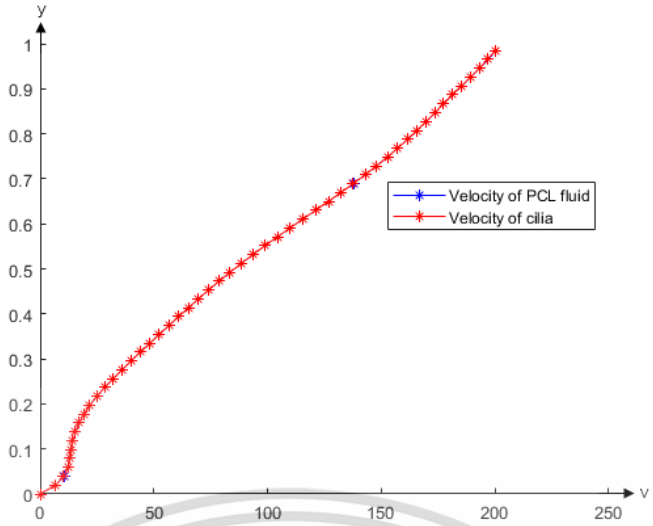

Figure 4.10: The velocity of the PCL fluid and the cilia velocity when $\theta = 80°$.

Table 4.7: Pointwise numerical solution and the velocity of cilia when cilia make angle $\theta = 80°$ with the horizontal plane.

y	0	0.1970	0.3939	0.5909	0.7878	0.9848
Numerical result	0	21.8073	60.8669	109.8793	161.5565	200.2622
Velocity of cilia	0	21.8319	60.8740	109.8826	161.5388	200.0000

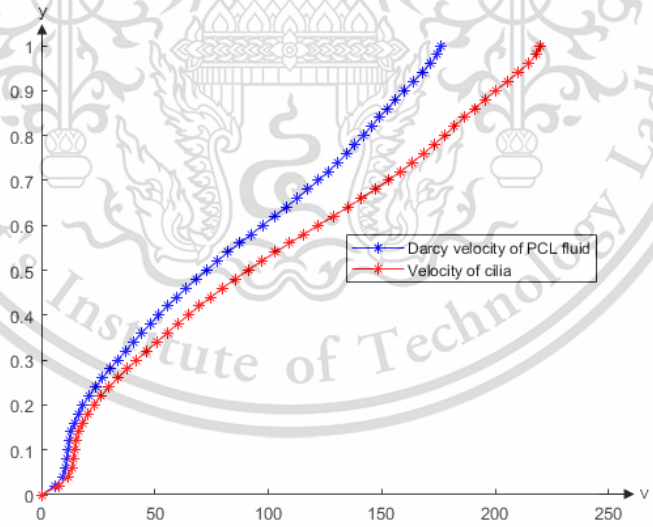

Figure 4.11: The Darcy velocity of PCL fluid and the cilia velocity when $\theta = 90°$.

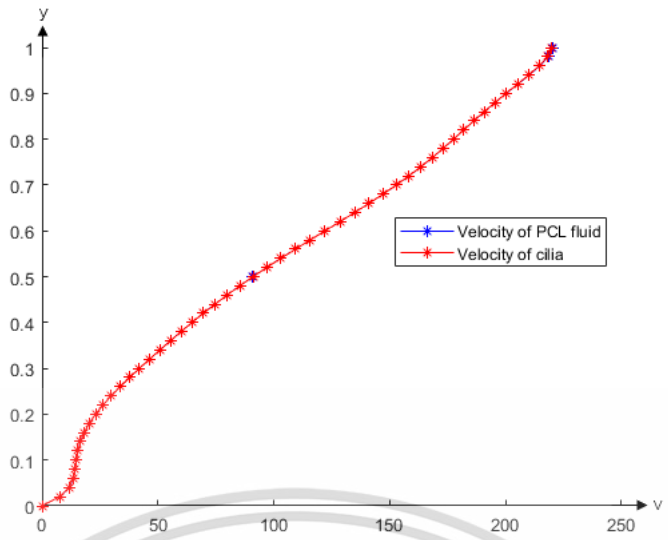

Figure 4.12: The velocity of PCL fluid and the cilia velocity when $\theta = 90°$.

Table 4.8: Pointwise numerical solution and the velocity of cilia when cilia make angle $\theta = 90°$ with the horizontal plane.

y	0	0.2	0.4	0.6	0.8	1.0
Numerical result	0	23.0744	64.6608	122.0917	177.5361	220.2753
Velocity of cilia	0	23.0849	64.6657	122.0911	177.5273	220

Table 4.9: The l_2-norm error of the numerical solutions when cilia make angle $\theta = 50°, 60°, ..., 90°$.

angle	l_2-norm error
50°	0.2828
60°	0.2800
70°	0.3924
80°	0.4078
90°	0.4623

Table 4.9 shows the the l_2-norm error of the numerical solutions when cilia make angle $\theta = 50°, 60°, ..., 90°$, we can see that the velocity of PCL fluid is closed to the velocity of cilia.

Figures 4.3, 4.4, 4.5 and 4.6 show that when $y < 0.1$, the velocities of the PCL fluid are negative because the velocity of the PCL fluid depends on the velocity of cilia. Figures 4.3, 4.5, 4.7, 4.9 and 4.11 show the Darcy velocity of the PCL fluid and the velocity of cilia. We can see that the velocity of the PCL fluid are constantly increase and the Darcy velocity of the PCL fluid is less than the velocity of cilia, which corresponds to the physical meaning.

Chapter 5

Conclusion

5.1 Conclusion

In this study, we consider the fluid flow in the Periciliary layer (PCL) containing cilia in the human lungs. When cilia efficiently move back and forward to precede the mucus out the human body, the cilia make an angle θ with the horizontal plane. When $\theta < 90°$, the region PCL is divided into 2 layers that are a free-fluid region and a porous medium. The PCL has only one domain, a porous medium, if cilia are perpendicular to the horizontal plane. We apply the Stokes-Brinkman equations in macroscopic scale embedding a nonlinear term with a moving solid phase to the problem. The Brinkman equation is employed in the porous region. The velocities of the cilia are added into the Brinkman equation as a source term since the PCL fluid moves by the ciliary beating instead of the pressure gradient. In this work, the nonlinear term is changed into a linear form by using a classical linearization method. We use the Galerkin finite element method to discretize the one-dimensional Stokes-Brinkman equations with the nonlinear term. The numerical results of this study are obtained by using a computer program. The numerical result of the Stokes-Brinkman equations is compared with an exact solution when there are no cilia velocity and also no nonlinear term in the governing equation. The numerical results of the nonlinear Stokes-Brinkman equations are compared with the velocity of cilia when cilia make angle, $\theta = 50°$ to $90°$, with the horizontal plane. We calculate the solutions by using 50 elements. The poisewise values of the numerical and exact solutions are shown in Table 4.2. The poisewise values of the numerical solutions and the velocities of the cilia are shown in Tables 4.3 to 4.11. The l_2-norm error of the numerical solution compare with the exact solution is 0.0072, which is in good agreement with the exact solution. The l_2-norm error of the velocity of the PCL fluid and the velocity of cilia are shown in Table 4.9. We can see that the velocity of PCL fluid is closed to the velocity of cilia. We compare the Darcy velocity of the PCL fluid with the velocity of the cilia, which can conclude that the velocity of the cilia is greater than the Darcy velocity of the PCL fluid, which is following the physical meaning.

References

[1] K. Chamsri. N-Dimensional Stokes-Brinkman Equations using a Mixed Finite Element Method. *Australian Journal of Basic and Applied Sciences*, 8:30–36, 2014.

[2] K. Chamsri. Formulation of a Well-Posed Stokes-Brinkman Problem with a Permeability Tensor. *Journal of Mathematics*, 1:1–7, 2015.

[3] M. Ciarletta, B. Straughan, and V. Tibullo. Modelling boundary and nonlinear effects in porous media flow. *Nonlinear Analysis: Real World Applications*, 12:2839–2843, 2011.

[4] H.N.E. Dine and M. Saad. Analysis of a finite volume-finite element method for Darcy-Brinkman two-phase flows in porous media. *Journal of Computational and Applied Mathematics*, 337:51–72, 2018.

[5] G.N. Gatica, L.F. Gatica, and F.A. Sequeira. Analysis of an augmented pseudostress-based mixed formulation for a nonlinear brinkman model of porous media flow. *Computer Methods in Applied Mechanics and Engineering*, 289:104–130, 2015.

[6] D. Han and X. Wang. Initial-boundary layer associated with the nonlinear Darcy-Brinkman system. *Differential Equation*, 256:609–639, 2014.

[7] J. Hussong, R. Lindken, P. Faulhammer, K. Noreikat, K.V. Sharp, W. Kummer, and J. Westerweel. Cilia-driven particle and fluid transport over mucus-free mice tracheae. *Biomechanics*, 46:593–598, 2013.

[8] P.G. Jayathilake, Z. Tan, D.V. Le, H.P. Lee, and B.C. Khoo. Three-dimensional numerical simulations of human pulmonary cilia in the periciliary liquid layer by the immersed boundary method. *Computers & Fluids*, 67:130–137, 2012.

[9] B.K. Jha and M.L. Kaurangini. Approximate Analytical Solutions for the Nonlinear Brinkman-Forchheimer-Extended Darcy Flow Model. *Applied Mathematics*, 2:1432–1436, 2011.

[10] Y.W. Kwon and H. Bang. *The Finite Element Method Using MATLAB Second Edition*. the United States of America, 2000.

[11] W.L. Lee, P.G. Jayathilake, Z. Tan, D.V. Le, H.P. Lee, and B.C. Khoo. Muco-ciliary transport: Effect of mucus viscosity, cilia beat frequency and cilia density. *Computers & Fluids*, 49:214–221, 2011.

[12] S. Suankasem, A. Pimkote, I. Thammathon, and K. Wuttanachamsri. Matched Asymptotic Expansion for PCL fluid Due to The movement of Lung cilia: Part 1. *10th National Science Research Conference*, 2018.

[13] K. Wuttanachamsri. Mucus Velocity in Human Lungs. *17th International Conference on Computation and Mathematical Methods in Science and Engineering*, 2017.

[14] K. Wuttanachamsri and L. Schreyer. Effects of the Cilia Movement on Fluid Velocity for Fixed Domain I: Mathematical Model, to be published.

[15] K. Wuttanachamsri and L. Schreyer. Effects of the Cilia Movement on Fluid Velocity for Fixed Domain II: Numerical Analysis, to be published.

Appendix

Appendix A

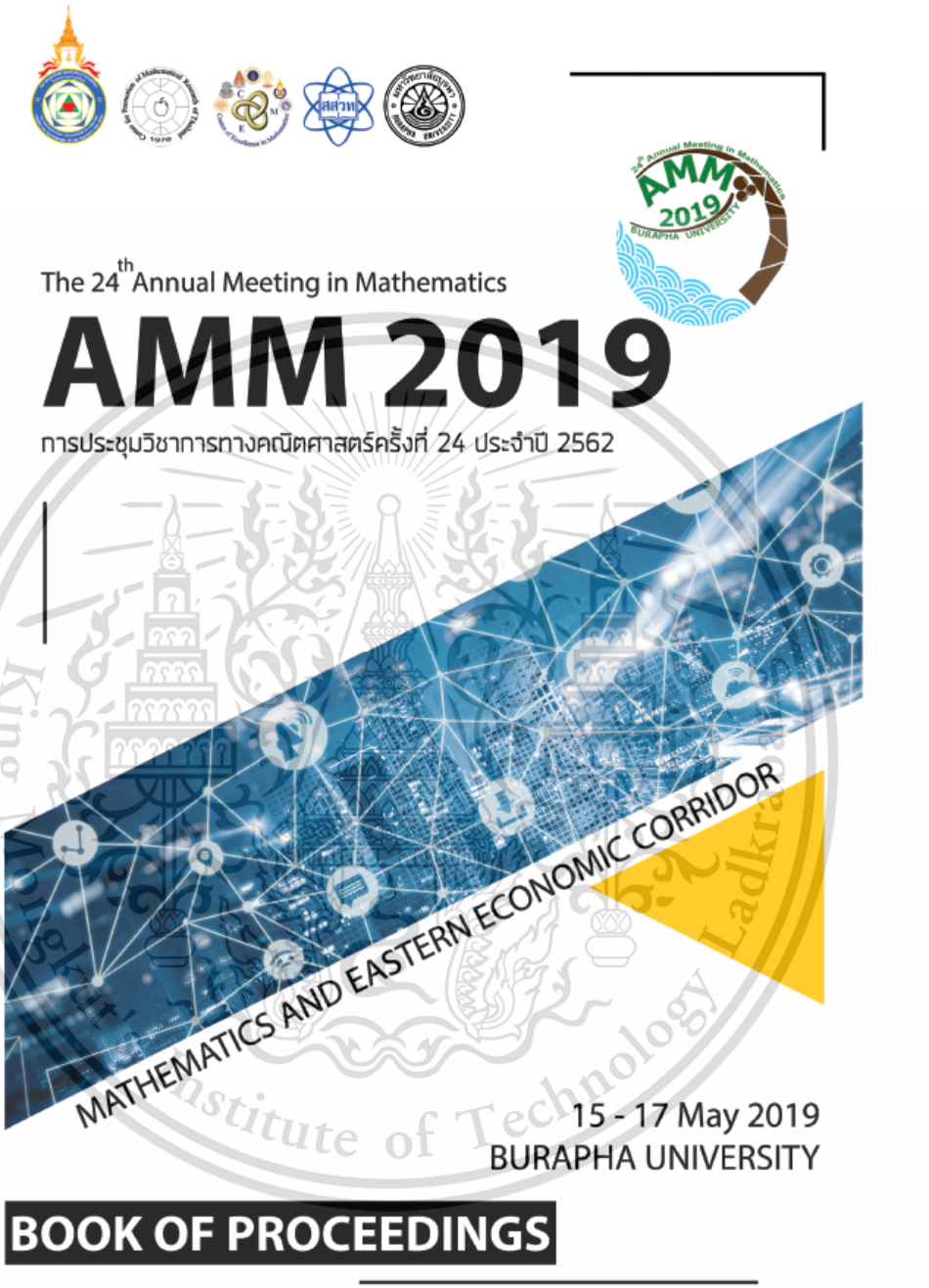

The 24th Annual Meeting in Mathematics (AMM 2019)

On the one-dimensional nonlinear Stokes-Brinkman equations for modeling flow in PCL

Surachai Phaenchat[1,*] and **Kanognudge Wuttanachamsri**[2]

Department of Mathematics, Faculty of Science, King Mongkut's Institute of Technology Ladkrabang, Bangkok, Thailand; [1]s.phaenchat@gmail.com; [2]whychamsri@hotmail.com
[*] Correspondence: s.phaenchat@gmail.com

Abstract: Nowadays, people have several respiratory diseases. One of the main reasons is the inhalation of strange particles such as dust and harmful smoke particles. When an irritant settles in the human body, goblet cells standing within a surface epithelium secrete mucus to catch those particles and then it forms a mucous layer and lies on the tip of cilia aligned along the ciliated epithelial cells. Then the mucus is moved out of the body by the movement of the cilia. The layer consisting of the hair-like structures and also a Newtonian fluid under the mucous layer is called Periciliary Layer (PCL). In order to study the velocity of the mucus, in this work, we first focus on the velocity of the fluid in the PCL so that it can be used as a boundary condition of the mucous layer. The Stokes-Brinkman equations embedding a nonlinear term is employed for solving this problem. The velocity of the cilia is also imposed in the model. The nonlinear structure is converted into a linear form by using a classical linearization method. In this research we discretize the model by using a finite element method where the numerical solutions will be provided in future work.

Keywords: moving solid phases; finite element method; Galerkin method; nonlinear Stoke-Brinkman equations

AMS Math Classification (2010) : 65P99, 92B05

1 Introduction

In the present days, there are several factors causing respiratory failure in human lungs such as factory pollutions. When people inhale the strange particles into their bodies, they spread directly into the respiratory tracts and lungs. This may cause respiratory diseases such as Pulmonary emphysema, Acute Bronchitis and Pneumonia. Some people who have the respiratory diseases have shortness of breath, cough and chest tightness. In this study, we focus on fluid flow in the respiratory system.

Figure 1 shows a portion of the respiratory tract: trachea, and its cross section.

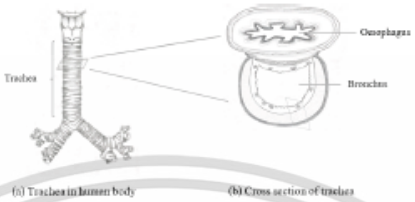

Figure 1: Trachea and its cross section.

A sector of the cross section of the trachea is illustrated in Figure 2 presenting ciliated cells, hair-like structures, goblet cells and mucus. Among the ciliated cells, there are goblet cells secreting the mucus to trap debris and form a mucus layer on the tip of the hair-like structures. Patients who have respiratory diseases may carry more mucous than usual. The tiny hair-like structures are named cilia, sticking out from the ciliated cells, that are efficiently move back and forward to precede the mucus out the body. The layer having of cilia and Newtonian fluid is called Periciliary Layer (PCL). To study the velocity of mucus, in this work, we first examine on the velocity of the fluid in PCL.

Figure 2: Cartoon figure of the portion of the cross section of trachea.

Numerous researchers had concentrated on the PCL [1, 2, 3]. For instance, J. Hussong et al. [1] studied cilia-induced periciliary liquid (PCL) transport measured by means of micro Particle Image Velocimetry (μPIV) with neutrally buoyant tracers. W.L. Lee et al. [3] numerically considered a two-layer Newtonian fluid model consisting of an upper mucus layer and a lower periciliary layer (PCL) to simulate the muco-ciliary transport process. P.G. Jayathilake et al. [2] presented a three-dimensional numerical model to simulate the human pulmonary cilia motion in the PCL. The governing equations were solved using the immersed boundary method combined with the projection method. The numerical results showed the maximum velocity of PCL in a stream-wise direction if cilia had phase differences in both stream-wise and span-wise directions.

When cilia make angle θ, which is less than 90° with the horizontal plane, the PCL can be split into 2 layers, hairy and hairless layers. Hairy layer is viewed as a porous medium and hairless layer is a free-fluid domain. We use Stokes-Brinkman equations in both of the domains. The Stokes equation is used in the free-fluid domain and Brinkman equation is used in the porous medium. In this work, we employ the Stokes-Brinkman model with a nonlinear term to find the velocity of the fluid in PCL. The Stokes-Brinkman equations without the nonlinear term in macroscopic scale had been developed in [4] and proved the well-posedness, when permeability coefficient was considered to be an n-dimensional tensor in [5]. The model was discretized in an n-dimensional domain in [6] by using a mixed finite element method. Next, K. Wuttanachamsri [7] employed the Stokes equation to find the mucus velocity by using a mixed finite element method in a three-dimensional domain.

Several literatures had been studied on the porous medium by using Brinkman or Darcy equations [8, 9, 10, 11]. For instant, Gabriel N. Gatica et al. [9] applied an augmented mixed finite element method for the two-dimensional nonlinear Brinkman model of a porous medium with mixed boundary conditions. S. Suankasem et al. [11] used a matched asymptotic expansion to the Brinkman equation and found the velocity of the PCL fluid

in a one-dimensional domain. Daozhi Han and Xiaoming Wang [10] applied the nonlinear Darcy-Brinkman system in the vanishing Darcy number limit and approximated solutions constructed by the method of multiple scale expansion in space and time. Houssein Nasser El Dine and Mazen Saad [8] interested in the displacement of two incompressible flow in porous media. Basant K. Jha and Muhammad L. Kaurangini [12] presented a new approximated analytical solution for steady flow in parallel-plates channels filled with porous materials governed by non-linear Brinkman-Forchheimer extended Darcy model for three different physical situations and the results were compared with those obtained from an implicit finite-difference solution. M. Ciarletta et al. [13] considered the problem of a Brinkman-Forchheimer system to model flow in a porous medium when Newton cooling conditions were applied at the boundary of the body.

However, most of the above literatures studied on static solid phases, except [6, 5, 11, 7]. Although Chamsri K. [6, 5], Wuttanachamsri K. [7] and Suankasem S. et al. [11] worked on moving solid phases, they used only linear models. In this work, the Stokes-Brinkman model with a nonlinear term including a moving solid-phase term is employed and discretized by using a finite element method. One of applications is that the velocity of the PCL fluid can be applied to be a boundary condition of the mucous layer.

The mathematical model is provided in Section 2. The nonlinear term is transformed into a linear form by using a classical linearization method in Section 3. Model discretization is presented in Section 4. and conclusion is drawn in Section 5.

2 Mathematical Model

In this section, we present the mathematical model used in this study. We consider this problem in a macroscale equation upscaled by the Hybrid Mixture Theory (HTM) [4]. It is an upscaling method that help to change a microscale equation to a macroscale equation. The macroscopic equation employ in this study is derived from Navier-Stokes equation in [4], which is

$$\frac{\partial}{\partial t}(\rho^l v) + \nabla \cdot \left(\rho^l v \frac{v}{\varepsilon^l}\right) + \varepsilon^l \nabla p - (\mu \Delta v + \mu \nabla(\nabla \cdot v)) - \varepsilon^l \rho^l g^l = -\mu \varepsilon^l \mathbf{k}^{-1} \cdot (v - \varepsilon^l v^s) \tag{1}$$

$$\nabla \cdot v = f \tag{2}$$

where $f = \dfrac{\dot{\varepsilon}^l}{(1-\varepsilon^l)} + \nabla \cdot \varepsilon^l v^s$; ρ^l is the fluid density; v is the multiplication of the fluid velocity with porosity in the PCL; ε^l is the porosity; p is pressure; μ is a dynamic viscosity; g^l is gravity; $\mathbf{k}^{-1}$ is the inverse of the permeability tensor; v^s is the velocities of the solid phases and $\dot{\varepsilon}^l$ is the material time derivative of the porosity with respect to the solid phase, $\dot{\varepsilon}^l = \dfrac{\partial \varepsilon^l}{\partial t} + v^s \cdot \nabla \varepsilon^l$. Substituting Eq. (2) into Eq. (1), we have

$$\frac{\partial}{\partial t}(\rho^l v) + \nabla \cdot \left(\rho^l v \frac{v}{\varepsilon^l}\right) + \varepsilon^l \nabla p - (\mu \Delta v + \mu \nabla f) - \varepsilon^l \rho^l g^l = -\mu \varepsilon^l \mathbf{k}^{-1} \cdot (v - \varepsilon^l v^s). \tag{3}$$

For one-dimensional domian, Eq. (3) can be rewritten as

$$\rho^l \frac{\partial v}{\partial t} + \frac{\rho^l}{\varepsilon^l} \frac{\partial v^2}{\partial y} + \varepsilon^l \frac{\partial p}{\partial x} - \mu \frac{\partial^2 v}{\partial y^2} - \mu \frac{\partial f}{\partial y} - \varepsilon^l \rho^l g^l = -\varepsilon^l \mu \mathbf{k}^{-1} \cdot v + \varepsilon^l \mu \mathbf{k}^{-1} \cdot (\varepsilon^l v^s), \tag{4}$$

where we assume that pressure p change in the x direction and $\dfrac{\partial p}{\partial x}$ is a constant and the fluid velocity depends on y direction. Rearranging Eq. (4), we have

$$\rho^l \frac{\partial v}{\partial t} + \frac{2\rho^l v}{\varepsilon^l} \frac{\partial v}{\partial y} - \mu \frac{\partial^2 v}{\partial y^2} + \varepsilon^l \mu \mathbf{k}^{-1} \cdot v = \varepsilon^l \mu \mathbf{k}^{-1} \cdot (\varepsilon^l v^s) + \varepsilon^l \rho^l g^l + \mu \frac{\partial f}{\partial y} - \varepsilon^l \frac{\partial p}{\partial x}, \tag{5}$$

where the right hand side of the equation are known. In this work, we interest in the steady state of Eq. (5), which is

$$\frac{2\rho^l v}{\varepsilon^l} \frac{\partial v}{\partial y} - \mu \frac{\partial^2 v}{\partial y^2} + \varepsilon^l \mu \mathbf{k}^{-1} \cdot v = \varepsilon^l \mu \mathbf{k}^{-1} \cdot (\varepsilon^l v^s) + \varepsilon^l \rho^l g^l + \mu \frac{\partial f}{\partial y} - \varepsilon^l \frac{\partial p}{\partial x}. \tag{6}$$

The solid velocity is employed from [14], which is a polynomial degree 8 depending on the length of cilia ξ,

$$v^s = c_8 \xi^8 + c_7 \xi^7 + c_6 \xi^6 + c_5 \xi^5 + c_4 \xi^4 + c_3 \xi^3 + c_2 \xi^2 + c_1 \xi^1 + c_0 \tag{7}$$

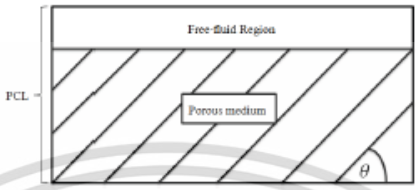

Figure 3: The cilia make the angle θ with the horizontal plane in PCL.

where $\xi = \dfrac{y}{\sin\theta}$ and the variable θ is the angle between the cilia and the horizontal plane as shown in Figure 3.

Then Eq. (6) becomes

$$\frac{2\rho^l v}{\varepsilon^l}\frac{\partial v}{\partial y} - \mu\frac{\partial^2 v}{\partial y^2} + \varepsilon^l\mu\mathbf{k}^{-1}\cdot v = \left(\varepsilon^l\right)^2\mu\mathbf{k}^{-1}c_8\left(\frac{y}{\sin\theta}\right)^8 + \left(\varepsilon^l\right)^2\mu\mathbf{k}^{-1}c_7\left(\frac{y}{\sin\theta}\right)^7 + \cdots + \left(\varepsilon^l\right)^2\mu\mathbf{k}^{-1}c_1\left(\frac{y}{\sin\theta}\right) + \left(\varepsilon^l\right)^2\mu\mathbf{k}^{-1}c_0 + \varepsilon^l\rho^l g^l + \mu\frac{\partial f}{\partial y} - \varepsilon^l\frac{\partial p}{\partial x}. \tag{8}$$

We now have the mathematical model with a nonlinear term, which is linearized in the next section.

3 Classical Linearization

We use classical linearization technique [15] to linearize the nonlinear term in Eq. (8) to be a linear form. The general form of an n^{th} order ordinary differential equation is

$$v^{(n)} + \Re\left(v, v', \ldots, v^{(n-1)}; y\right) + \aleph\left(v, v', \ldots, v^{(n-1)}; y\right) = f(y) \tag{9}$$

where $v^{(n)}$ is the n^{th} derivative of v; $\Re$ is the linear differential operator and $\aleph$ is the nonlinear differential operator.

The basic idea of classical linearization is to linearize a nonlinear differential equations to be a linear equation by acting on v or its derivatives. The classical linearization of $\aleph$ is acquired by approximation

$$\aleph \approx \ell^* = \left(\frac{\aleph^*}{\Im^*}\right)\Im \tag{10}$$

where linear differential operator ℓ^* is function of previous values of v which change during the iterative process; $\aleph^*$ and $\Im^*$ are evaluated from known values of the arguments from previous iterations and $\Im$ is a linear operator, which may have more than one form.

The classical linearization for Eq. (8) is given below

$$v'v \approx (v')^* v = \Im^* \tag{11}$$

$$v'v \approx v^*(v') = \Im^* \tag{12}$$

where v^* is an approximation of v and $(v')^*$ is the approximation of the first derivative of approximation of v.

4 Model Discritization

In this section, we discretize our governing equation provided in Section 2 by using the Galerkin finite element method.

Since the momentum equation has a nonlinear term, we apply the classical linearization to change it to be linear by substituting Eq. (11) into Eq. (8). Then, we have

$$\frac{2\rho^l}{\varepsilon^l}(v')^* v - \mu\frac{\partial^2 v}{\partial y^2} + \varepsilon^l\mu\mathbf{k}^{-1}\cdot v = \left(\varepsilon^l\right)^2\mu\mathbf{k}^{-1}c_8\left(\frac{y^8}{\sin^8\theta}\right) + \left(\varepsilon^l\right)^2\mu\mathbf{k}^{-1}c_7\left(\frac{y^7}{\sin^7\theta}\right) + \cdots + \left(\varepsilon^l\right)^2\mu\mathbf{k}^{-1}c_1\left(\frac{y}{\sin\theta}\right) + \left(\varepsilon^l\right)^2\mu\mathbf{k}^{-1}c_0 + \varepsilon^l\rho^l g^l + \mu\frac{\partial f}{\partial y} - \varepsilon^l\frac{\partial p}{\partial x}. \tag{13}$$

Next, we find the weak formulation of the model by multiplying Eq. (13) by a weight function $w \in H_0^1(\Omega)$ and then integrating over the domain $\Omega = [0, L]$. Therefore Eq. (13) becomes

$$\int_0^L \left(\frac{2\rho^l}{\varepsilon^l}(v')^* wv - \mu w \frac{\partial^2 v}{\partial y^2} + \varepsilon^l \mu \mathbf{k}^{-1} wv \right) dy = \int_0^L \left(\left(\varepsilon^l\right)^2 \mu \mathbf{k}^{-1} c_8 \left(\frac{wy^8}{\sin^8 \theta} \right) + \left(\varepsilon^l\right)^2 \mu \mathbf{k}^{-1} c_7 \left(\frac{wy^7}{\sin^7 \theta} \right) + \cdots \right.$$
$$\left. + \left(\varepsilon^l\right)^2 \mu \mathbf{k}^{-1} c_1 \left(\frac{wy}{\sin \theta} \right) + \left(\varepsilon^l\right)^2 \mu \mathbf{k}^{-1} c_0 w + \varepsilon^l \rho^l g^l w + \mu w \frac{\partial f}{\partial y} - \varepsilon^l w \frac{\partial p}{\partial x} \right) dy. \tag{14}$$

We apply integration by parts to the second order derivative and term of $\partial f / \partial y$ in Eq. (14) and discretize the domain to be n elements. Then, we have

$$\sum_{i=1}^{n} \int_{y_i}^{y_{i+1}} \left(\frac{2\rho^l}{\varepsilon^l}(v')^* wv + \mu \frac{\partial w}{\partial y} \frac{\partial v}{\partial y} + \varepsilon^l \mu \mathbf{k}^{-1} wv \right) dy = \sum_{i=1}^{n} \int_{y_i}^{y_{i+1}} \left(\left(\varepsilon^l\right)^2 \mu \mathbf{k}^{-1} c_8 \left(\frac{wy^8}{\sin^8 \theta} \right) \right.$$
$$\left. + \left(\varepsilon^l\right)^2 \mu \mathbf{k}^{-1} c_7 \left(\frac{wy^7}{\sin^7 \theta} \right) + \left(\varepsilon^l\right)^2 \mu \mathbf{k}^{-1} c_1 \left(\frac{wy}{\sin \theta} \right) + \cdots + \left(\varepsilon^l\right)^2 \mu \mathbf{k}^{-1} c_0 w + \varepsilon^l \rho^l g^l w - \mu f \frac{\partial w}{\partial y} - \varepsilon^l w \frac{\partial p}{\partial x} \right) dy$$
$$+ \mu \left[wf \right]_0^L + \mu \left[wv' \right]_0^L. \tag{15}$$

Consider the first integration,

$$\int_{y_i}^{y_{i+1}} \left(\frac{2\rho^l}{\varepsilon^l}(v')^* wv + \mu \frac{\partial w}{\partial y} \frac{\partial v}{\partial y} + \varepsilon^l \mu \mathbf{k}^{-1} wv \right) dy. \tag{16}$$

We assume that

$$v^* = y.$$

Then

$$(v')^* = 1.$$

Using linear shape functions

$$H_1 = \frac{y_{i+1} - y}{h_i}$$
$$H_2 = \frac{y - y_i}{h_i}, \tag{17}$$

where $h_i = y_{i+1} - y_i$, we obtain

$$v = H_1 v_1 + H_2 v_2 \tag{18}$$

or in the matrix form

$$v = \begin{bmatrix} H_1 & H_2 \end{bmatrix} \begin{bmatrix} v_1 \\ v_2 \end{bmatrix}. \tag{19}$$

Replacing the weight function w by the linear shape function Eq. (17) and substituing Eq. (19) into Eq. (16), we have the 2×2 matrix

$$[K_e] = \int_{y_i}^{y_{i+1}} \left(\frac{2\rho^l}{\varepsilon^l} \begin{bmatrix} H_1 \\ H_2 \end{bmatrix} \begin{bmatrix} H_1 & H_2 \end{bmatrix} \begin{bmatrix} v_i \\ v_{i+1} \end{bmatrix} + \mu \begin{bmatrix} H_1' \\ H_2' \end{bmatrix} \begin{bmatrix} H_1' & H_2' \end{bmatrix} \begin{bmatrix} v_i \\ v_{i+1} \end{bmatrix} \right.$$
$$\left. + \varepsilon^l \mu \mathbf{k}^{-1} \begin{bmatrix} H_1 \\ H_2 \end{bmatrix} \begin{bmatrix} H_1 & H_2 \end{bmatrix} \begin{bmatrix} v_i \\ v_{i+1} \end{bmatrix} \right) dy$$
$$[K_e] = \int_{y_i}^{y_{i+1}} \left(\frac{2\rho^l}{\varepsilon^l} \begin{bmatrix} H_1 H_1 & H_1 H_2 \\ H_2 H_1 & H_2 H_2 \end{bmatrix} + \mu \begin{bmatrix} H_1' H_1' & H_1' H_2' \\ H_2' H_1' & H_2' H_2' \end{bmatrix} + \varepsilon^l \mu \mathbf{k}^{-1} \begin{bmatrix} H_1 H_1 & H_1 H_2 \\ H_2 H_1 & H_2 H_2 \end{bmatrix} \right) dy \begin{bmatrix} v_i \\ v_{i+1} \end{bmatrix}$$

Define

$$[K_e] = \begin{bmatrix} k_{11} & k_{12} \\ k_{21} & k_{22} \end{bmatrix}. \tag{20}$$

The elements k_{ij} in $[K_e]$ can be calculated as follows. Consider

$$
\begin{aligned}
k_{11} &= \int_{y_i}^{y_{i+1}} \frac{2\rho^l}{\varepsilon^l} H_1 H_1 + \mu H_1' H_1' + \varepsilon^l \mu \mathbf{k}^{-1} H_1 H_1 \, dy \\
&= \int_{y_i}^{y_{i+1}} \frac{2\rho^l}{\varepsilon^l} \left(\frac{y_{i+1}-y}{h_i}\right)^2 + \mu \left(\frac{-1}{h_i}\right)^2 + \varepsilon^l \mu \mathbf{k}^{-1} \left(\frac{y_{i+1}-y}{h_i}\right)^2 dy \\
&= \int_{y_i}^{y_{i+1}} \frac{2\rho^l}{\varepsilon^l} \left(\frac{y_{i+1}^2 - 2y_{i+1}y + y^2}{h_i^2}\right) + \left(\frac{\mu}{h_i^2}\right) + \varepsilon^l \mu \mathbf{k}^{-1} \left(\frac{y_{i+1}^2 - 2y_{i+1}y + y^2}{h_i^2}\right) dy \\
&= \frac{2\rho^l}{\varepsilon^l h_i^2} \left(y_{i+1}^2 y - 2y_{i+1}\frac{y^2}{2} + \frac{y^3}{3}\right)\Bigg|_{y_i}^{y_{i+1}} + \left(\frac{\mu}{h_i^2}\right)(y)\Bigg|_{y_i}^{y_{i+1}} + \frac{\varepsilon^l \mu \mathbf{k}^{-1}}{h_i^2} \left(y_{i+1}^2 y - 2y_{i+1}\frac{y^2}{2} + \frac{y^3}{3}\right)\Bigg|_{y_i}^{y_{i+1}} \\
&= \frac{2\rho^l}{\varepsilon^l h_i^2} \left(\frac{y_{i+1}^3 - 3y_{i+1}^2 y_i + 3y_{i+1}y_i^2 - y_i^3}{3}\right) + \frac{\mu}{h_i^2}(y_{i+1} - y_i) \\
&+ \frac{\varepsilon^l \mu \mathbf{k}^{-1}}{h_i^2} \left(\frac{y_{i+1}^3 - 3y_{i+1}^2 y_i + 3y_{i+1}y_i^2 - y_i^3}{3}\right) \\
&= \frac{2\rho^l}{\varepsilon^l h_i^2} \left(\frac{(y_{i+1}-y_i)^3}{3}\right) + \frac{\mu}{h_i^2}(y_{i+1} - y_i) + \frac{\varepsilon^l \mu \mathbf{k}^{-1}}{h_i^2} \left(\frac{(y_{i+1}-y_i)^3}{3}\right) \\
&= \frac{2\rho^l}{\varepsilon^l h_i^2} \left(\frac{h_i^3}{3}\right) + \frac{\mu}{h_i^2}(h_i) + \frac{\varepsilon^l \mu \mathbf{k}^{-1}}{h_i^2} \left(\frac{h_i^3}{3}\right) \\
&= \frac{2\rho^l h_i}{3\varepsilon^l} + \frac{\mu}{h_i} + \frac{\varepsilon^l \mu \mathbf{k}^{-1} h_i}{3}.
\end{aligned}
$$

Thus,

$$
k_{11} = \frac{2\rho^l h_i}{3\varepsilon^l} + \frac{\mu}{h_i} + \frac{\varepsilon^l \mu \mathbf{k}^{-1} h_i}{3}. \tag{21}
$$

Consider

$$
\begin{aligned}
k_{12} &= \int_{y_i}^{y_{i+1}} \frac{2\rho^l}{\varepsilon^l} H_1 H_2 + \mu H_1' H_2' + \varepsilon^l \mu \mathbf{k}^{-1} H_1 H_2 \, dy \\
&= \int_{y_i}^{y_{i+1}} \frac{2\rho^l}{\varepsilon^l} \left(\frac{y_{i+1}-y}{h_i}\right)\left(\frac{y-y_i}{h_i}\right) + \mu\left(\frac{-1}{h_i}\right)\left(\frac{1}{h_i}\right) + \varepsilon^l\mu\mathbf{k}^{-1}\left(\frac{y_{i+1}-y}{h_i}\right)\left(\frac{y-y_i}{h_i}\right) dy \\
&= \int_{y_i}^{y_{i+1}} \frac{2\rho^l}{\varepsilon^l} \left(\frac{y_{i+1}y - y_{i+1}y_i - y^2 + y_i y}{h_i^2}\right) - \left(\frac{\mu}{h_i^2}\right) + \varepsilon^l\mu\mathbf{k}^{-1}\left(\frac{y_{i+1}y - y_{i+1}y_i - y^2 + y_i y}{h_i^2}\right) dy \\
&= \frac{2\rho^l}{\varepsilon^l h_i^2}\left(y_{i+1}\frac{y^2}{2} - y_{i+1}y_i y - \frac{y^3}{3} + y_i\frac{y^2}{2}\right)\Bigg|_{y_i}^{y_{i+1}} - \left(\frac{\mu}{h_i^2}\right)(y)\Big|_{y_i}^{y_{i+1}} \\
&+ \frac{\varepsilon^l\mu\mathbf{k}^{-1}}{h_i^2}\left(y_{i+1}\frac{y^2}{2} - y_{i+1}y_i y - \frac{y^3}{3} + y_i\frac{y^2}{2}\right)\Bigg|_{y_i}^{y_{i+1}} \\
&= \frac{2\rho^l}{\varepsilon^l h_i^2}\left(\frac{y_{i+1}^3}{2} - y_{i+1}^2 y_i - \frac{y_{i+1}^3}{3} + y_i\frac{y_{i+1}^2}{2} - y_{i+1}\frac{y_i^2}{2} + y_{i+1}y_i^2 + \frac{y_i^3}{3} - \frac{y_i^3}{2}\right) - \frac{\mu}{h_i^2}(y_{i+1}-y_i) \\
&+ \frac{\varepsilon^l\mu\mathbf{k}^{-1}}{h_i^2}\left(\frac{y_{i+1}^3}{2} - y_{i+1}^2 y_i - \frac{y_{i+1}^3}{3} + y_i\frac{y_{i+1}^2}{2} - y_{i+1}\frac{y_i^2}{2} + y_{i+1}y_i^2 + \frac{y_i^3}{3} - \frac{y_i^3}{2}\right) \\
&= \frac{2\rho^l}{\varepsilon^l h_i^2}\left(\frac{y_{i+1}^3 - 3y_{i+1}^2 y_i + 3y_{i+1}y_i^2 - y_i^3}{6}\right) - \frac{\mu}{h_i^2}(y_{i+1}-y_i) \\
&+ \frac{\varepsilon^l\mu\mathbf{k}^{-1}}{h_i^2}\left(\frac{y_{i+1}^3 - 3y_{i+1}^2 y_i + 3y_{i+1}y_i^2 - y_i^3}{6}\right) \\
&= \frac{2\rho^l}{\varepsilon^l h_i^2}\left(\frac{(y_{i+1}-y_i)^3}{6}\right) - \frac{\mu}{h_i^2}(y_{i+1}-y_i) + \frac{\varepsilon^l\mu\mathbf{k}^{-1}}{h_i^2}\left(\frac{(y_{i+1}-y_i)^3}{6}\right) \\
&= \frac{2\rho^l}{\varepsilon^l h_i^2}\left(\frac{h_i^3}{6}\right) - \frac{\mu}{h_i^2}(h_i) + \frac{\varepsilon^l\mu\mathbf{k}^{-1}}{h_i^2}\left(\frac{h_i^3}{6}\right) \\
&= \frac{\rho^l h_i}{3\varepsilon^l} - \frac{\mu}{h_i} + \frac{\varepsilon^l\mu\mathbf{k}^{-1}h_i}{6}.
\end{aligned}
$$

Thus,

$$k_{12} = \frac{\rho^l h_i}{3\varepsilon^l} - \frac{\mu}{h_i} + \frac{\varepsilon^l\mu\mathbf{k}^{-1}h_i}{6} = k_{21}. \tag{22}$$

and

$$
\begin{aligned}
k_{22} &= \int_{y_i}^{y_{i+1}} \frac{2\rho^l}{\varepsilon^l} H_2 H_2 + \mu H_2' H_2' + \varepsilon^l\mu\mathbf{k}^{-1} H_2 H_2 \, dy \\
&= \int_{y_i}^{y_{i+1}} \frac{2\rho^l}{\varepsilon^l}\left(\frac{y-y_i}{h_i}\right)^2 + \mu\left(\frac{1}{h_i}\right)^2 + \varepsilon^l\mu\mathbf{k}^{-1}\left(\frac{y-y_i}{h_i}\right)^2 dy \\
&= \int_{y_i}^{y_{i+1}} \frac{2\rho^l}{\varepsilon^l}\left(\frac{y^2 - 2yy_i + y_i^2}{h_i^2}\right) + \left(\frac{\mu}{h_i^2}\right) + \varepsilon^l\mu\mathbf{k}^{-1}\left(\frac{y^2 - 2yy_i + y_i^2}{h_i^2}\right) dy \\
&= \frac{2\rho^l}{\varepsilon^l h_i^2}\left(\frac{y^3}{3} - 2\frac{y^2}{2}y_i + y_i^2 y\right)\Bigg|_{y_i}^{y_{i+1}} + \left(\frac{\mu}{h_i^2}\right)(y)\Big|_{y_i}^{y_{i+1}} + \frac{\varepsilon^l\mu\mathbf{k}^{-1}}{h_i^2}\left(\frac{y^3}{3} - 2\frac{y^2}{2}y_i + y_i^2 y\right)\Bigg|_{y_i}^{y_{i+1}} \\
&= \frac{2\rho^l}{\varepsilon^l h_i^2}\left(\frac{y_{i+1}^3 - 3y_{i+1}^2 y_i + 3y_{i+1}y_i^2 - y_i^3}{3}\right) + \frac{\mu}{h_i^2}(y_{i+1}-y_i) \\
&+ \frac{\varepsilon^l\mu\mathbf{k}^{-1}}{h_i^2}\left(\frac{y_{i+1}^3 - 3y_{i+1}^2 y_i + 3y_{i+1}y_i^2 - y_i^3}{3}\right)
\end{aligned}
$$

$$k_{22} = \frac{2\rho^l}{\varepsilon^l h_i^2}\left(\frac{(y_{i+1}-y_i)^3}{3}\right) + \frac{\mu}{h_i^2}(y_{i+1}-y_i) + \frac{\varepsilon^l \mu \mathbf{k}^{-1}}{h_i^2}\left(\frac{(y_{i+1}-y_i)^3}{3}\right)$$
$$= \frac{2\rho^l}{\varepsilon^l h_i^2}\left(\frac{h_i^3}{3}\right) + \frac{\mu}{h_i^2}(h_i) + \frac{\varepsilon^l \mu \mathbf{k}^{-1}}{h_i^2}\left(\frac{h_i^3}{3}\right)$$
$$= \frac{2\rho^l h_i}{3\varepsilon^l} + \frac{\mu}{h_i} + \frac{\varepsilon^l \mu \mathbf{k}^{-1} h_i}{3}.$$

Thus,

$$k_{22} = \frac{2\rho^l h_i}{3\varepsilon^l} + \frac{\mu}{h_i} + \frac{\varepsilon^l \mu \mathbf{k}^{-1} h_i}{3}. \tag{23}$$

Next, we consider the right hand side forms of Eq. (15):

$$\sum_{i=1}^{n}\int_{y_i}^{y_{i+1}}\left(\left(\varepsilon^l\right)^2\mu\mathbf{k}^{-1}c_8\left(\frac{wy^8}{\sin^8\theta}\right) + \left(\varepsilon^l\right)^2\mu\mathbf{k}^{-1}c_7\left(\frac{wy^7}{\sin^7\theta}\right) + \cdots + \left(\varepsilon^l\right)^2\mu\mathbf{k}^{-1}c_1\left(\frac{wy}{\sin\theta}\right)\right.$$
$$\left. + \left(\varepsilon^l\right)^2\mu\mathbf{k}^{-1}c_0 w + \varepsilon^l\rho^l g^l w - \mu f\frac{\partial w}{\partial y} - \varepsilon^l w\frac{\partial p}{\partial x}\right)dy + \mu[wf]_0^L + \mu\left[wv'\right]_0^L. \tag{24}$$

Define the vector

$$[f_e] = \int_{y_i}^{y_{i+1}}\left(\left(\varepsilon^l\right)^2\mu\mathbf{k}^{-1}c_8\frac{y^8}{\sin^8\theta}\begin{bmatrix}H_1\\H_2\end{bmatrix} + \left(\varepsilon^l\right)^2\mu\mathbf{k}^{-1}c_7\frac{y^7}{\sin^7\theta}\begin{bmatrix}H_1\\H_2\end{bmatrix} + \cdots + \left(\varepsilon^l\right)^2\mu\mathbf{k}^{-1}c_1\frac{y}{\sin\theta}\begin{bmatrix}H_1\\H_2\end{bmatrix}\right.$$
$$\left. + \left(\varepsilon^l\right)^2\mu\mathbf{k}^{-1}c_0\begin{bmatrix}H_1\\H_2\end{bmatrix} + \varepsilon^l\rho^l g^l\begin{bmatrix}H_1\\H_2\end{bmatrix} + \mu f\begin{bmatrix}H_1'\\H_2'\end{bmatrix} - \varepsilon^l\frac{\partial p}{\partial x}\begin{bmatrix}H_1\\H_2\end{bmatrix}\right)dy + \mu[wf]_0^L + \mu\left[wv'\right]_0^L. \tag{25}$$

where the variables in Eq. (25) are known which can be calculated by coding in a computer program.

5 Conclusion

In this study, we consider the fluid flow in the Periciliary layer (PCL) containing cilia. When cilia make angle θ, which is less than 90°, with the horizontal plane, the region PCL is divided into 2 layers that are a free-fluid region and a porous medium as shown in Figure 3. The PCL has only one domain, a porous medium, if cilia is perpendicular to the horizontal plane. We apply the Stokes-Brinkman equations in macroscopic scale embedding a nonlinear term with a moving solid phase to the problem. The macroscale equations are derived by using Hybrid Mixture Theory (HTM). The Brinkman equation is employed in the porous region while the Stokes equation is applied in the free-fluid domain. The velocity of cilia is added into the Brinkman equation as a source term since the PCL fluid moves by the ciliary beating instead of the pressure gradient. In this work, the nonlinear term is changed into a linear form by using a classical linearization method. We use the Galerkin finite element method to discretize the one-dimensional Stokes-Brinkman equations with the nonlinear term. The numerical solutions of this study will be provided in future work.

References

[1] Hussong J, Lindken R, Faulhammer P, Noreikat K, Sharp KV, Kummer W, et al. Cilia-driven particle and fluid transport over mucus-free mice tracheae. Biomechanics. 2013;46:593–598.

[2] Jayathilake PG, Tan Z, Le DV, Lee HP, Khoo BC. Three-dimensional numerical simulations of human pulmonary cilia in the periciliary liquid layer by the immersed boundary method. Computers & Fluids. 2012;67:130–137.

[3] Lee WL, Jayathilake PG, Tan Z, Le DV, Lee HP, Khoo BC. Muco-ciliary transport: Effect of mucus viscosity, cilia beat frequency and cilia density. Computers & Fluids. 2011;49:214–221.

[4] Wuttanachamsri K, Schreyer L. Effects of the Cilia Movement on Fluid Velocity for Fixed Domain I: Mathematical Model, to be published;.

[5] Chamsri K. Formulation of a Well-Posed Stokes-Brinkman Problem with a Permeability Tensor. Journal of Mathematics. 2015;1:1–7.

[6] Chamsri K. N-Dimensional Stokes-Brinkman Equations using a Mixed Finite Element Method. Australian Journal of Basic and Applied Sciences. 2014;8:30–36.

[7] Wuttanachamsri K. Mucus Velocity in Human Lungs. 17th International Conference on Computation and Mathematical Methods in Science and Engineering. 2017;.

[8] Dine HNE, Saad M. Analysis of a finite volume-finite element method for Darcy-Brinkman two-phase flows in porous media. Journal of Computational and Applied Mathematics. 2018;337:51–72.

[9] Gatica GN, Gatica LF, Sequeira FA. Analysis of an augmented pseudostress-based mixed formulation for a nonlinear Brinkman model of porous media flow. Computer Methods in Applied Mechanics and Engineering. 2015;289:104–130.

[10] Han D, Wang X. Initial-boundary layer associated with the nonlinear Darcy-Brinkman system. Differential Equation. 2014;256:609–639.

[11] Suankasem S, Pimkote A, Thammathon I, Wuttanachamsri K. Matched Asymptotic Expansion for PCL fluid Due to The movement of Lung cilia: Part 1. 10th National Science Research Conference. 2018;.

[12] Jha BK, Kaurangini ML. Approximate Analytical Solutions for the Nonlinear Brinkman-Forchheimer-Extended Darcy Flow Model. Applied Mathematics. 2011;2:1432–1436.

[13] Ciarletta M, Straughan B, Tibullo V. Modelling boundary and nonlinear effects in porous media flow. Nonlinear Analysis: Real World Applications. 2011;12:2839–2843.

[14] Wuttanachamsri K, Schreyer L. Effects of the Cilia Movement on Fluid Velocity for Fixed Domain II: Numerical Analysis, to be published;.

[15] Kwon YW, Bang H. The Finite Element Method Using MATLAB Second Edition. the United States of America; 2000.

Author Biography

Name	Mr.Surachai Phaenchat
Date of Birth	01 July 1995
Address	38/2, Chattrakan, Chattrakan District Phitsanulok Province, 65170
Education	2016 Bachelor of Science and Technology in Mathematics GPA 3.61 Rajamangala University of Technology Thanyaburi 2018 Master of Science in Applied Mathematics GPA 3.76 King Mongkut's Institute of Technology Ladkrabang

Academic Publication(s)

1. Surachai Phaenchat and Kanognudge Wuttanachamsri, "On the Nonlinear Stokes-Brinkman Equations for Modeling Flow in PCL.", Proceeding of Anual Meeting in Mathematics 2019. (AMM2019), May, 15-17, 2019, Burapha University, Chonburi, Thailand.